NASA/TP—1998–208396

Application of Rapid Prototyping Methods to High-Speed Wind Tunnel Testing

(MSFC Center Director's Discretionary Fund Final Report, Project No. 96–21)

A.M. Springer
Marshall Space Flight Center, Marshall Space Flight Center, Alabama

National Aeronautics and
Space Administration

Marshall Space Flight Center

May 1998

Acknowledgments

The author would like to thank the wind tunnel test team and rapid prototyping team at Marshall for their contributions in the wind tunnel test and model fabrication program. Many thanks to Henry Brewster, Holly Walker, Alonzo Frost, Mindy Niedermeyer, Ken Cooper, David Hoppe, and Floyd Roberts.

Available from:

NASA Center for AeroSpace Information
800 Elkridge Landing Road
Linthicum Heights, MD 21090–2934
(301) 621–0390

National Technical Information Service
5285 Port Royal Road
Springfield, VA 22161
(703) 487–4650

TABLE OF CONTENTS

LIST OF FIGURES

LIST OF TABLES

NOMENCLATURE

α	angle-of-attack
β	angle-of-sideslip
C_A	axial force coefficient
C_N	normal force coefficient
C_M	pitching moment coefficient
C_Y	side force coefficient
C_{YN}	yawing moment coefficient
$C_{\ell\beta}$	rolling moment coefficient
L_{ref}	reference length
S_{ref}	reference area
L/D	lift over drag ratio
X_{MRP}	moment reference point

ACRONYMS AND ABBREVIATIONS

ABS	acrylonitrile butadiene styrene
Al	aluminum
CAD	computer aided design
CDDF	Center Director's Discretionary Fund
FDM	fused deposition method
LOM	laminated object method
MSFC	Marshall Space Flight Center
NC	numerically controlled
PEEK	Poly Ether Ether Keytone
RP	rapid prototyping
SLA	stereolithography
SLS	selective laser sintering
TWT	Trisonic Wind Tunnel

TECHNICAL PUBLICATION

APPLICATION OF RAPID PROTOTYPING METHODS TO HIGH-SPEED WIND TUNNEL TESTING

I. INTRODUCTION

In a time when "better, faster, cheaper" are the words to live by, new technologies must be employed to try and live up to these axioms. In this spirit, a study has been undertaken to determine the suitability of models constructed using rapid prototyping (RP) methods for use in subsonic, transonic, and supersonic wind tunnel testing. This study was conducted to determine if the level of development in rapid prototyping materials and processes is adequate for constructing models, and if these models meet the structural requirements of subsonic, transonic, and supersonic testing while still having the high fidelity required to produce accurate aerodynamic data.

Initially a brief proof-of-concept or precursor study was undertaken to determine if rapid prototyping models showed any promise in this application. The study involved the construction of a fused deposition model to replicate the geometry of a model (fig.1) already slated for testing in the Marshall Space Flight Center's (MSFC's) 14-Inch Trisonic Wind Tunnel (TWT). This allowed a brief 20-run study which provided the necessary data to compare the aerodynamic characteristics of an RP model to that of a standard steel-machined model. The findings from this initial study indicated that the aerodynamic database obtained from RP models showed good agreement with data obtained from the machined steel counterpart. This warranted a more complete study using the various rapid prototyping methods against a more intricate model.

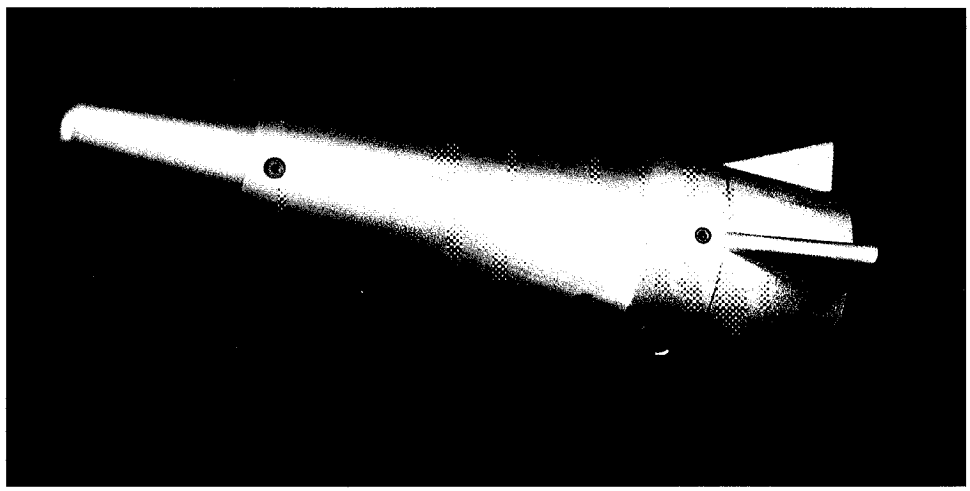

FIGURE 1.—Vertical lander model configuration.

A study funded through an MSFC Center Director's Discretionary Fund (CDDF) project was undertaken to determine the feasibility of using models constructed from rapid prototyping materials using RP methods for preliminary aerodynamic assessment of future launch vehicle configurations. This study was conducted to determine if certain criteria can be satisfactorily met in order to produce an adequate assessment of vehicle aerodynamic characteristics. These pertinent questions or criteria were as follows: (1) could RP methods be used to produce a detailed scale model within required dimensional tolerances; (2) did the available RP materials have the mechanical characteristics, strength, and elongation properties required to survive wind tunnel testing at subsonic, transonic, and supersonic speeds and still produce accurate data; (3) which RP process or processes and materials produce the best results; (4) what steps and methods are required to convert an RP model to a wind tunnel model (i.e., fitting a balance adapter into an RP model and attaching the model parts together); and (5) what are the costs and time requirements for the various RP methods as compared to a standard machined metal model?

RP models constructed using four methods and six materials were compared to a machined metal model. The RP processes were: fused deposition method (FDM) using materials of both acrylonitrile butadiene styrene (ABS) plastic and Poly Ether Ether Keytone (PEEK); stereolithography (SLA) with a photopolymer resin of STL–5170; selective laser sintering (SLS) with glass reinforced nylon as a material; and laminated object method (LOM) using both plastic reinforced with glass fibers and "paper." Aluminum (Al) was chosen as the material for the machined metal model. An aluminum model, while not as preferred as a steel model, costs less and requires less time to construct, thus providing a more conservative baseline model.

It can initially be stated that at the time of the study, machined metal models cannot be replaced by RP models for all required aspects of wind tunnel testing. This study focused on a small aspect of wind tunnel testing—determining the static stability aerodynamic characteristics of a vehicle relevant to preliminary vehicle configuration design.

While some of the RP methods or processes had reached a mature level of development, such as SLA, LOM using "paper," and FDM using ABS plastic, others still were in the development phase or were trying new materials which promised greater material properties or higher part definition. For this test, some of the materials and processes still in the development phase were tested. This provided some models which did not meet visual standards and were not converted into wind tunnel models. Two of these methods/materials were FDM using PEEK and LOM using a plastic reinforced with glass fibers. FDM is now a standard RP technique, but using PEEK as a material is still in the early testing phases. PEEK provides models with much greater strength, but at this time the surface finish and tolerances on the model were unacceptable. LOM is a newer method which normally uses "paper" to construct a model, but this has low material properties (i.e., it is likely to break under the loads expected while testing). A new LOM material, plastic, is being tested to provide higher properties. At the current time, this material shrinks 3 percent during curing. From the model received, this 3 percent is not consistent over the model since the model was warped and pitted. Due to these defects, this model was not converted to a wind tunnel test article. The LOM "paper" model was converted into a wind tunnel model, but the material delaminated during the process due to the loads experienced during the machining of the bore hole and the installation of the balance adapter. The other three RP methods tested were SLA, SLS, and FDM–ABS.

II. GEOMETRY

A. Precursor Study

The geometry used for the precursor study was that of a vertical lander concept (fig. 1). The vertical lander was a generic blunted cone followed by a bread-loaf-shaped base with two fins, or fairings, on the base's upper surface. Because this model was being fabricated in a machined metal model format (fig. 2), a preliminary computer aided design (CAD) file was available for RP model design and fabrication. This geometry provided a basis for comparisons between RP models and machined metal models. The reference dimensions for this configuration were as follows:

Vertical Lander
S_{ref}=4.957 in^2
L_{ref}=9.0 in
X_{MRP}=6.246 inches aft of nose

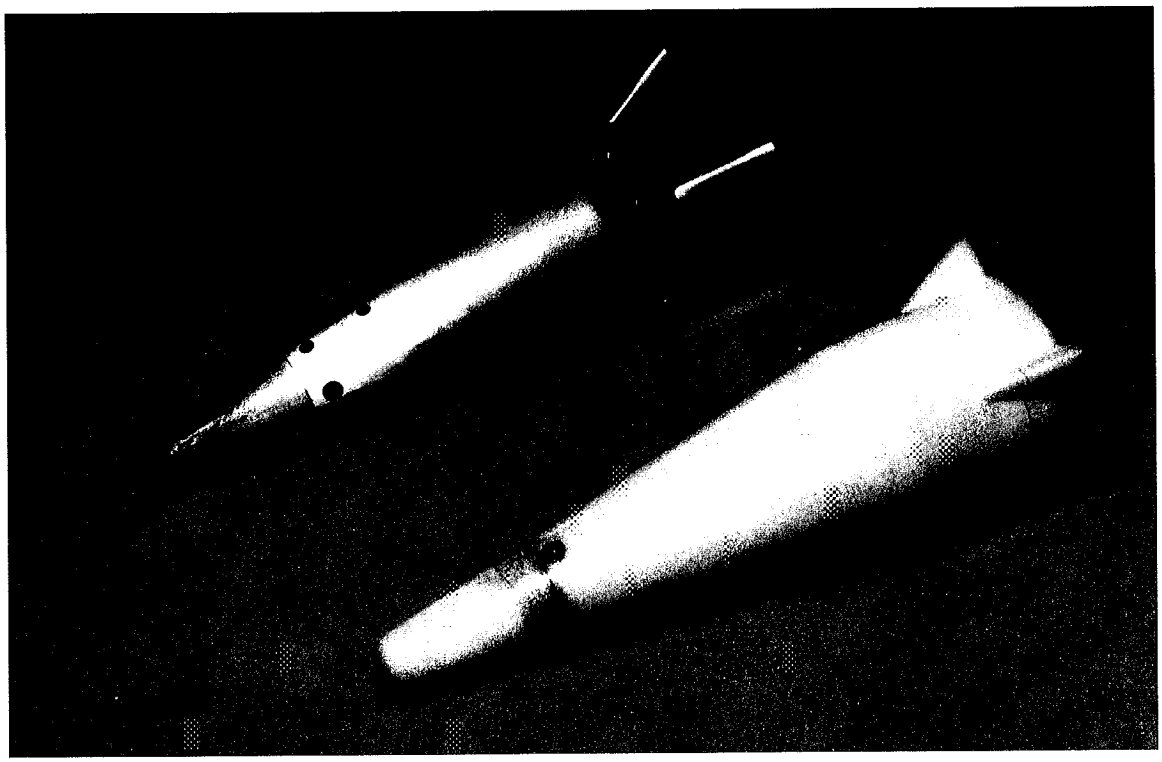

FIGURE 2.—Photograph of both steel and FDM–ABS vertical lander configurations.

B. Baseline Study

A wing-body-tail configuration was chosen for the actual study. First, this configuration would indicate possible deflections in the wings or tail due to loads and whether the manufacturing accuracy of the airfoil sections would adversely affect the aerodynamic data that resulted during testing. Secondly, will the model be able to withstand the starting, stopping and operating loads in a blowdown wind tunnel. The wing-body-tail configuration is shown in figure 3. The reference dimensions for this configuration are as follows:

Wing Body
S_{ref}=8.68 in^2
L_{ref}=8.922 in
X_{MRP}=6.2454 inches aft of nose

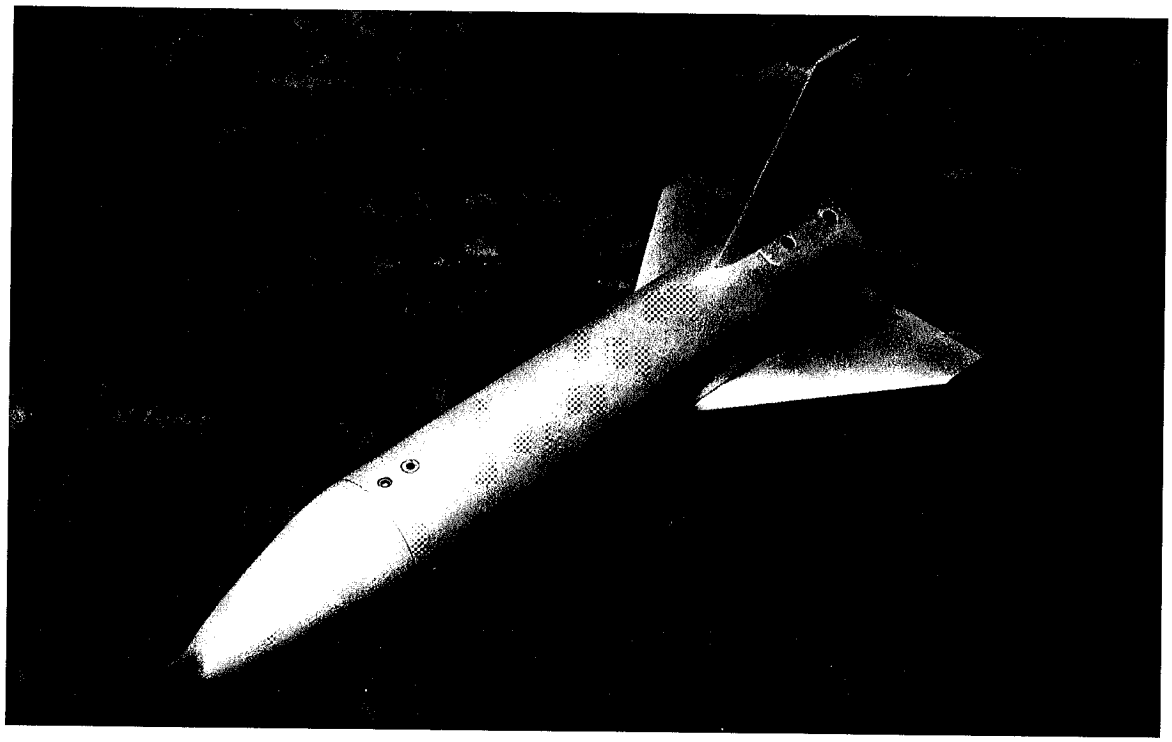

FIGURE 3.—Wing-body-tail configuration.

III. MODEL CONSTRUCTION

A. Precursor Study

The precursor study vertical lander RP model was constructed using the fused deposition method. The fused deposition method involves the layering of molten beaded ABS plastic material via a movable nozzle in 0.01-inch-thick layers. The model was constructed in two parts, a nose and a core body. A 0.75-inch hole was reamed through the center of the body for placement of the aluminum balance adapter, which was then epoxied into place (fig. 4). The nose was attached to the core body with a removable knock pin.

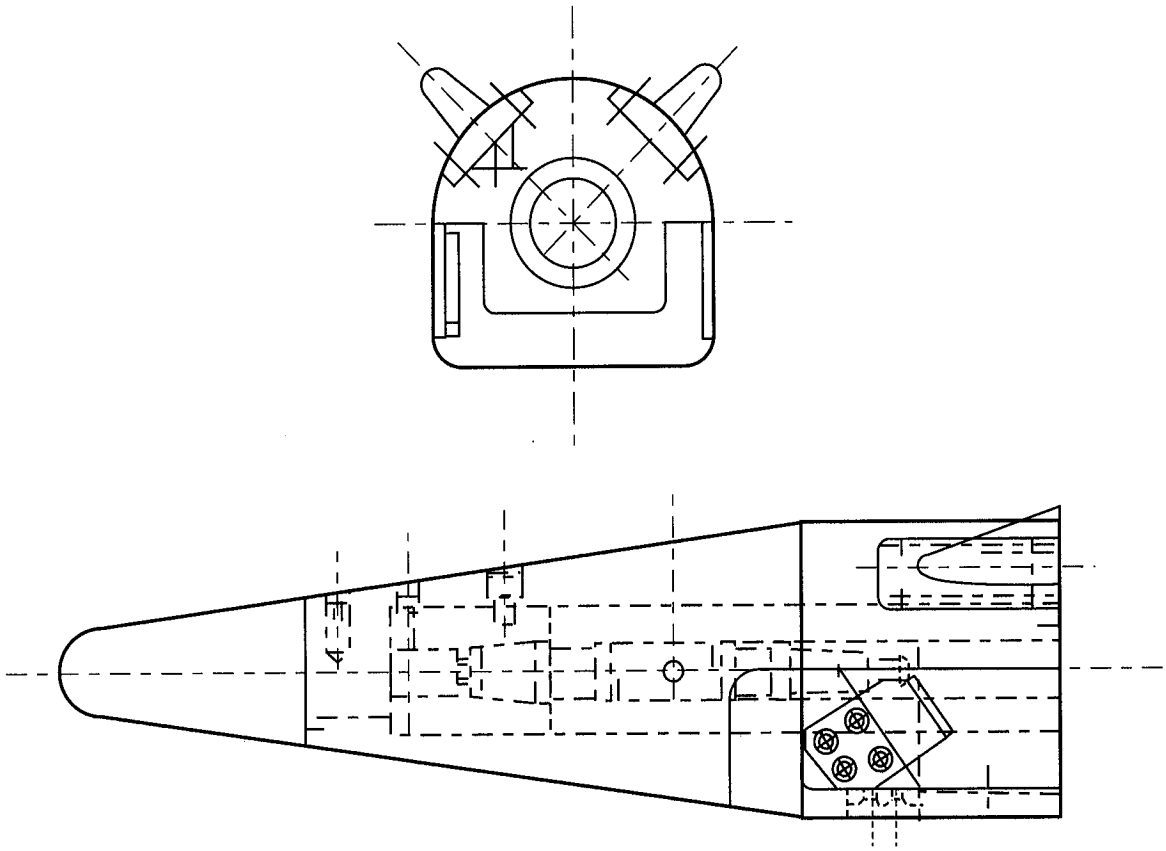

FIGURE 4.—Layout of vertical lander model geometry.

B. Baseline Study

The rapid prototyping processes and materials selected for the baseline study were the following:

- FDM–ABS by Stratasys using ABS plastic
- FDM–PEEK using carbon fiber reinforced PEEK
- SLA by Three-Dimensional Systems using SLA–5170
- SLS by DTM Technologies using glass-reinforced nylon
- LOM by Helisys using a glass-reinforced plastic and wood.

The RP models were constructed using the above materials and processes and are shown in figures 5 and 6. Figure 5 shows the models tested—aluminum, FDM–ABS, SLA, and SLS; while figure 6 shows the models which were not tested—LOM using plastic and wood.

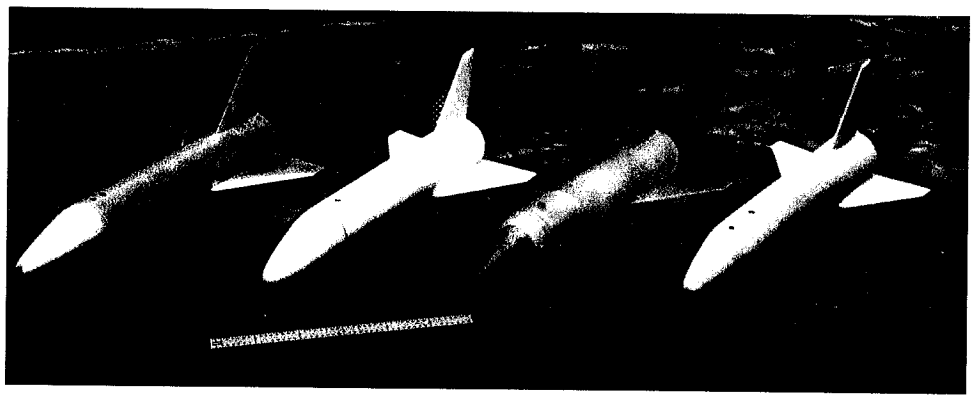

FIGURE 5.—Wing-body models tested (left to right), aluminum, FDM–ABS, SLA, and SLS.

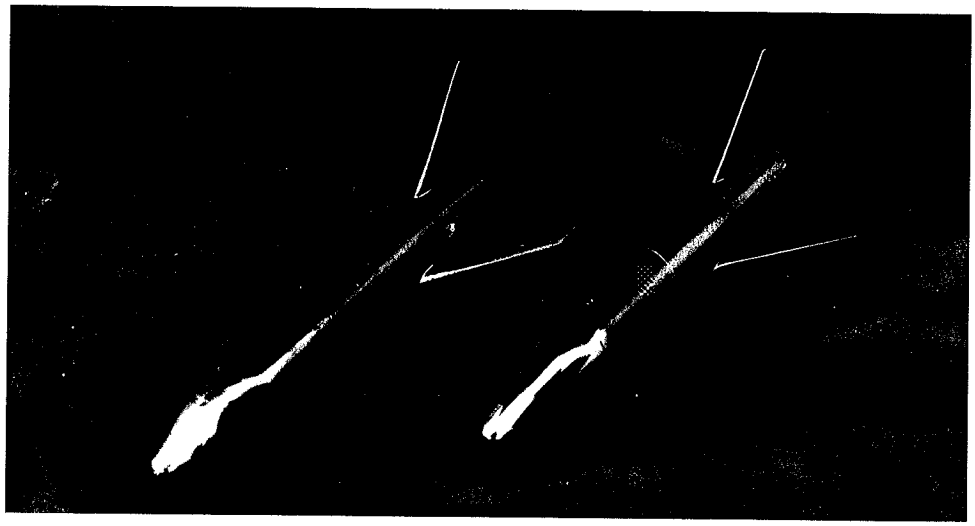

FIGURE 6.—The two LOM wing-body models (left to right), plastic and wood.

The fused deposition method involves the layering of molten beaded ABS plastic material via a movable nozzle in 0.01-inch-thick layers. The ABS material is supplied in rolls of thin ABS line resembling weed trimmer line. The material is heated and extruded through a nozzle similar to that of a hot glue gun. The plastic is deposited in rows and layered forming the part from numerically controlled (NC) data (fig. 7). The material PEEK is currently being studied for the FDM process.

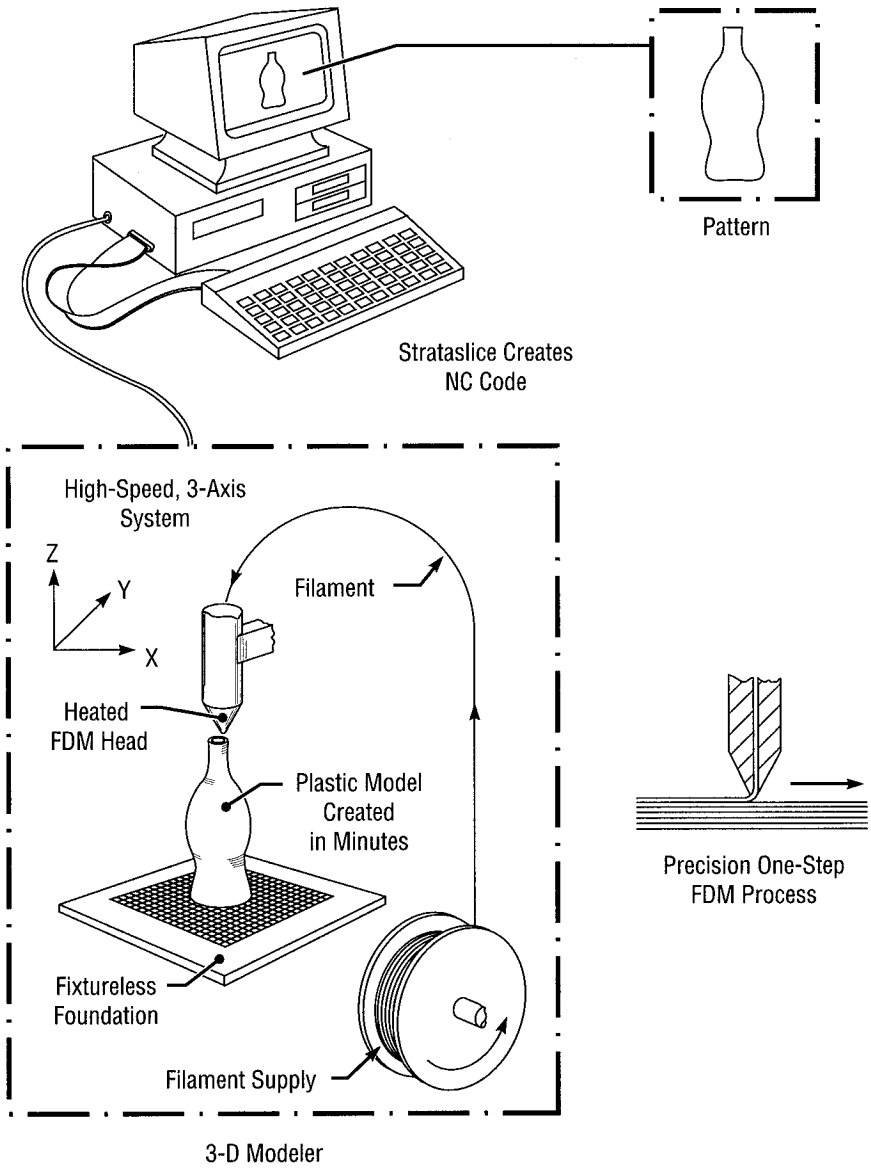

FIGURE 7.—The fused deposition method (FDM) rapid prototyping process.

Stereolithography uses a vat of a photopolymer epoxy resin which solidifies when hit by a UV laser (fig. 8). The laser solidifies each layer as the tray is lowered. This continues until the part is complete.

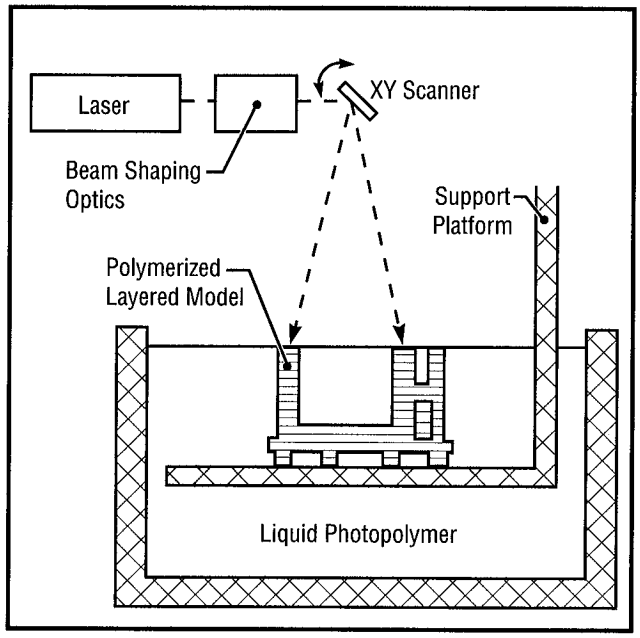

FIGURE 8.—The stereolithography (SLA) process.

Selective laser sintering uses a laser to fuse or sinter powdered glass and nylon particles or granules in layers which are fused on top of each other as with the other processes (fig. 9).

The SLS Process

1. A very thin layer of heat-fusible powder is deposited on top of the build cylinder.

2. Laser "draws" a cross-section that matches the corresponding layer in the STL file, bonding the particles and fusing the adjacent layers.

3. Roller mechanism deposits another powder layer.

4. Support platform moves the part downward a layer at a time and the process repeats, until the part is fully formed.

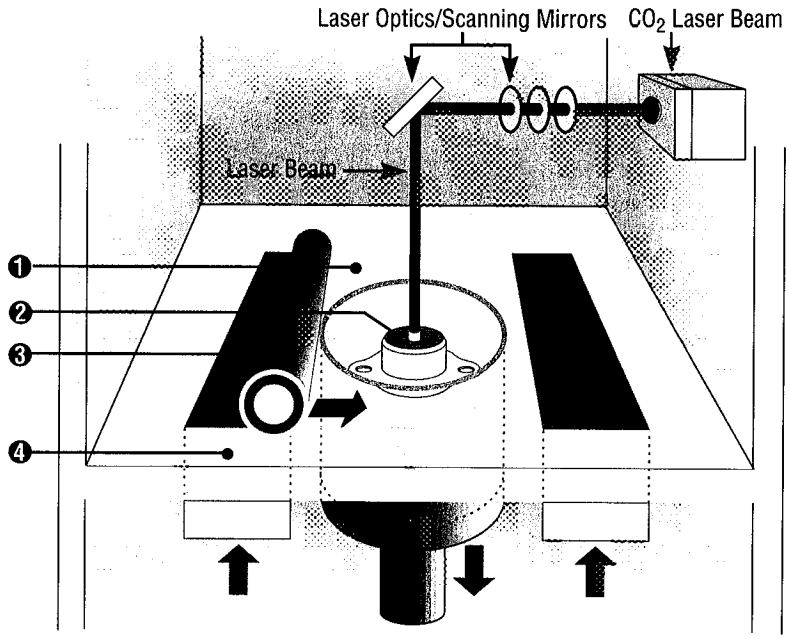

FIGURE 9.—The selective laser sintering (SLS) process.

Laminated object manufacturing involves rolling sheets of paper onto a machine equipped with a laser that cuts the pattern for each layer out of the paper. The next sheet is rolled on top of the previous one and the cutting procedure is repeated. The sheets have epoxy on one side which, when heated by a hot roller, fuses adjacent layers together. The model is built up in this fashion (fig. 10). Plastic currently is being tested to replace the use of paper or wood, due to its better materials properties.

The material properties of SLA, FDM–ABS, and SLS are shown in table 1, while aluminum and steel are shown in table 2.

TABLE 1.—*Material properties of SLA, FDM–ABS, and SLS.*

Property	Units	SLA SL5170	SLS Protoform	FDM–ABS
Tensile Strength	psi	8,700	7,100	5,000
Tensile Modulus	ksi	575	408	360
Elongation at Break	percent	12	6	50
Flexural Strength	psi	15,600	—	9,500
Flexural Modulus	ksi	429	625	380
Impact Strength	ft-lb/in	0.6	1.25	2
Hardness	(Shore D)	85	—	105

TABLE 2.—*Material properties of aluminum.*

Property	Aluminum 2024–T4	Aluminum 5086–H32	Steel 17–4PH H900
Yield Strength (ksi)	40	28	170
Tensile Strength (ksi)	62	40	190

Each of the RP models were constructed as a single part. The nose section was separated from the core and a 0.75-inch hole was drilled and reamed through the center of the body for placement of the aluminum balance adapter, which was then epoxied and pinned into place. The nose was attached to the core body with two screws which were attached through the nose to the balance adapter. Figure 11 shows an FDM model as built directly from the machine and still on its stand, a finished model with its nose removed, and an aluminum balance adapter as used in the models. Figure 12 is a close-up of an aluminum balance adapter.

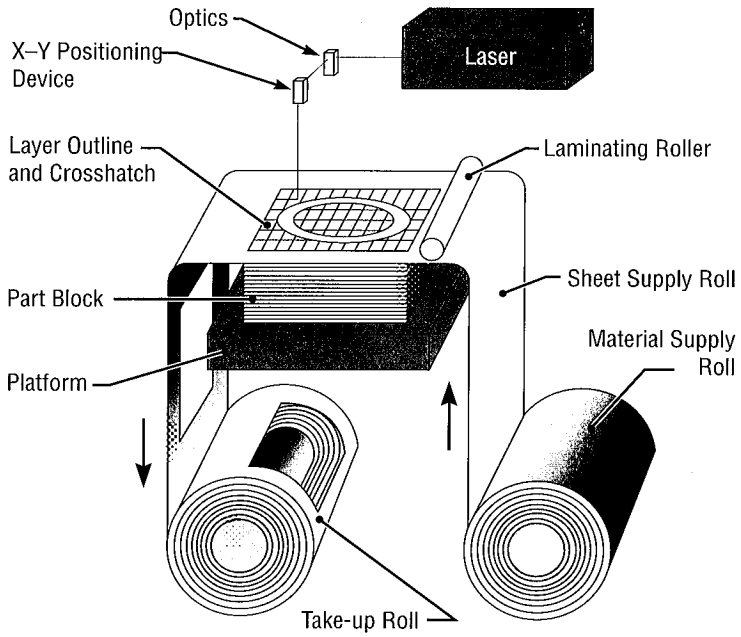

LOM Process

CAD data go into the LOM system's process controller and a cross-sectional slice is created by the LOM software.

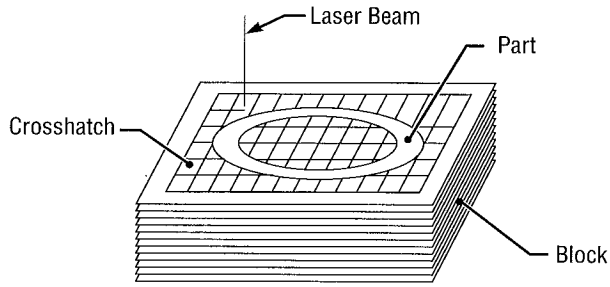

The laser cuts the cross-sectional outline in the top layer and then cross-hatches the excess material for later removal.

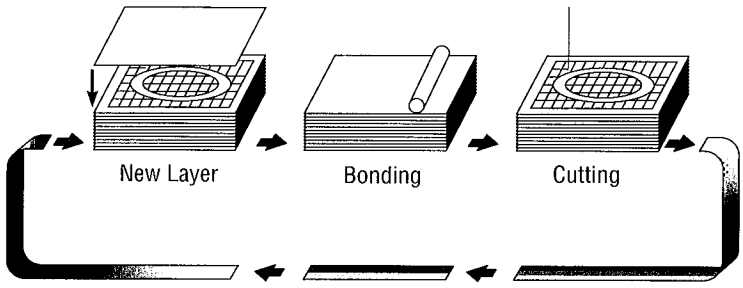

A new layer is bonded to the previously cut layer and a new cross section is created and cut as before. Once all layers have been laminated and cut, excess material is removed to expose the finished model.

FIGURE 10.—The laminated object manufacturing (LOM) process.

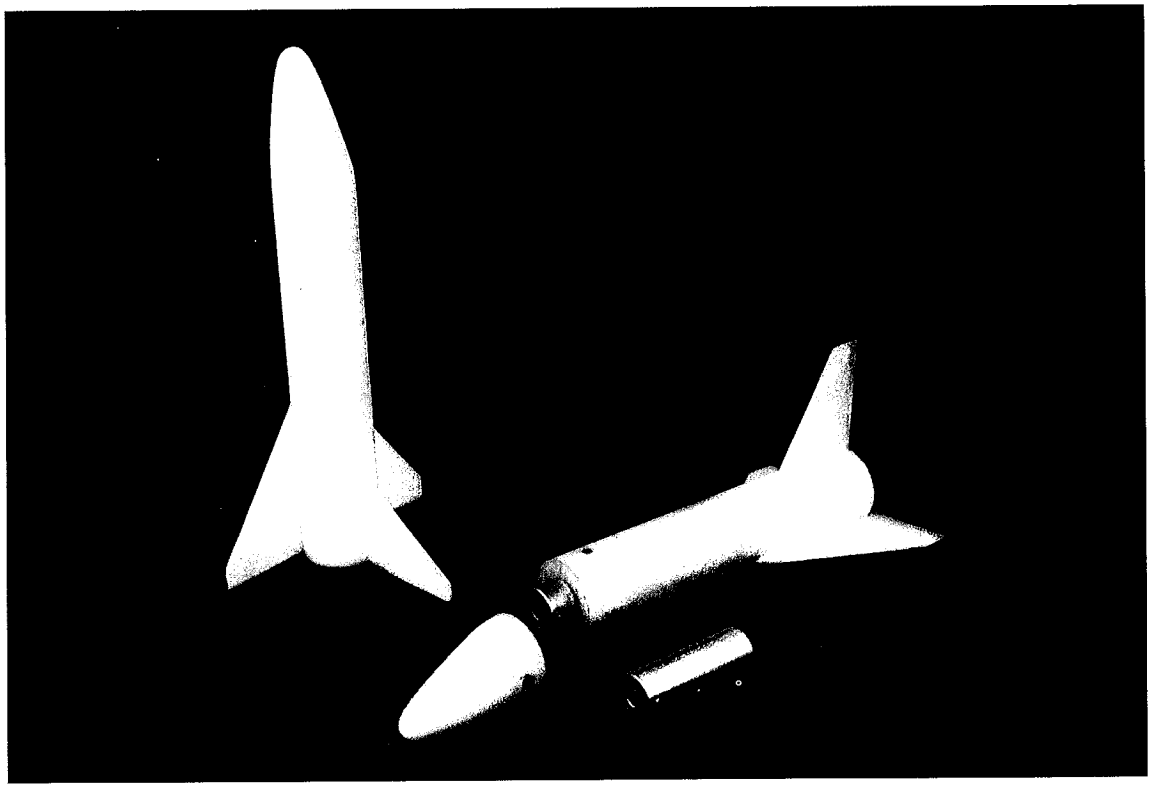

FIGURE 11.—Fused deposition method model straight from the machine, with fabrication stand, model converted into wind tunnel model, and aluminum balance adapter.

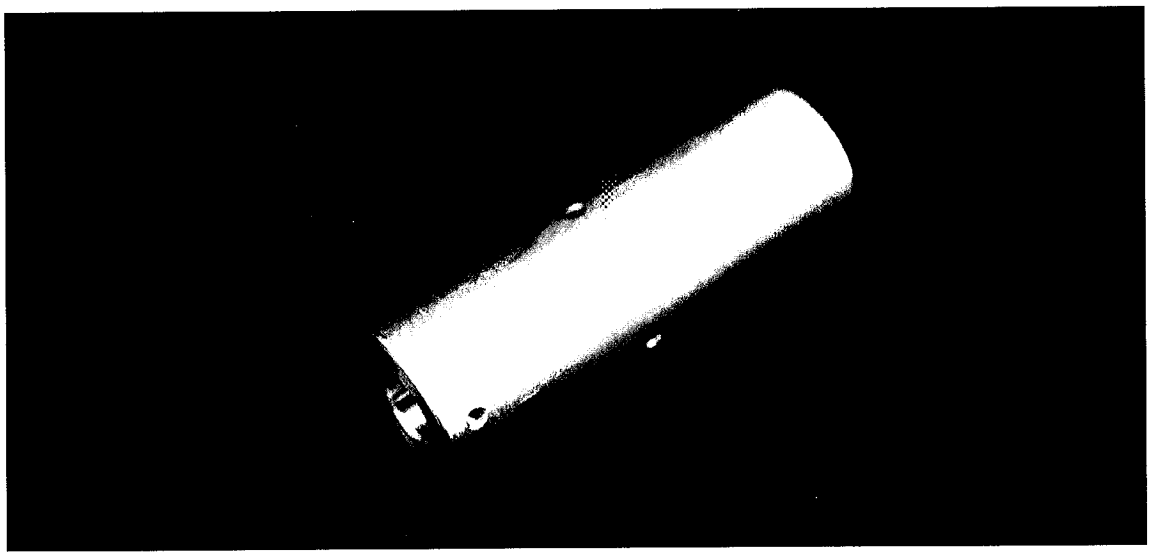

FIGURE 12.—Aluminum balance adapter used in models.

IV. FACILITY

The MSFC 14×14-Inch Trisonic Wind Tunnel (fig. 13) is an intermittent blowdown tunnel which operates by high-pressure air flowing from storage to either vacuum or atmosphere conditions. The transonic test section provides a Mach number range from 0.2 to 2.0. Mach numbers between 0.2 and 0.9 are obtained by using a controllable diffuser. The Mach range from 0.95 to 1.3 is achieved through the use of plenum suction and perforated walls. Each Mach number above 1.3 requires a specific set of two-dimensional contoured nozzle blocks. A solid wall supersonic test section provides the entire range from 2.74 to 5.0 with one set of movable fixed-contour nozzle blocks.

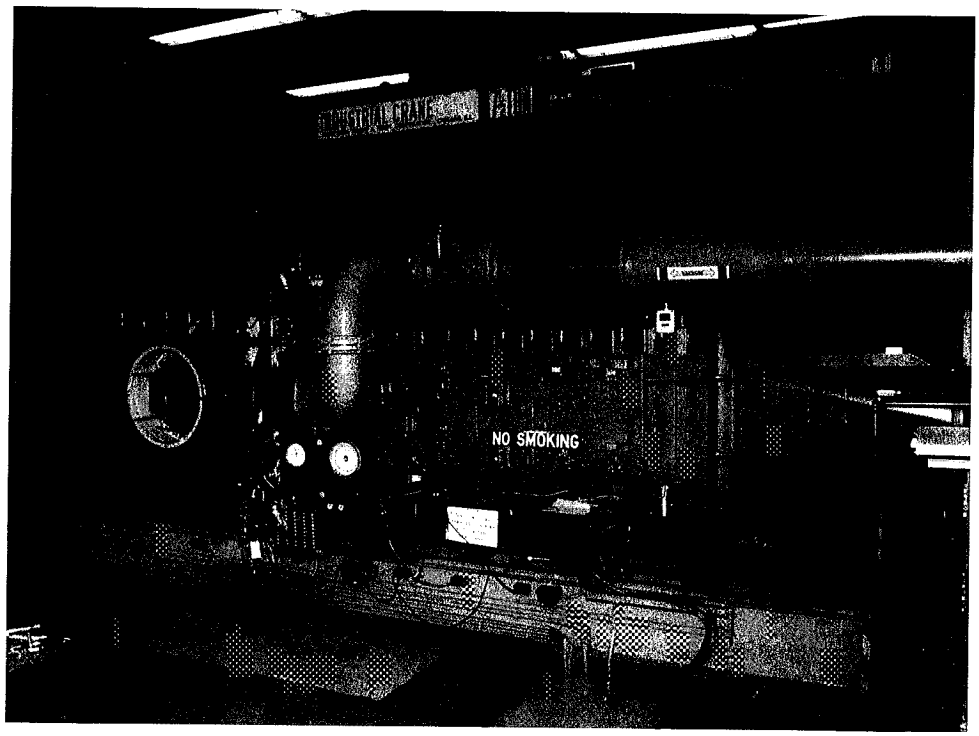

FIGURE 13.— Marshall Space Flight Center's 14×14-Inch Trisonic Wind Tunnel.

A three-stage reciprocating compressor driven by a 1,500 horsepower motor supplies air to a 6,000 ft^3 storage tank at approximately −40 °F dewpoint and 425 psig.

The tunnel flow is established and controlled with a servo-actuated gate valve. The controlled air flows through the valve diffuser into the stilling chamber and heat exchanger where the air temperature can be controlled from ambient to approximately 180 °F. The air then passes through the test section which contains the nozzle blocks and test region. Downstream of the test section is a hydraulically controlled pitch sector that provides the capability of testing angles-of-attack ranging from −10 to +10 degrees during each run. Sting offsets are available for obtaining various maximum angles-of-attack up to 90 degrees.

The diffuser section has movable floor and ceiling panels which are the primary means of controlling the subsonic Mach numbers and permit more efficient supersonic operation.

Tunnel flow is exhausted through an acoustically damped tower to atmosphere or into the vacuum field volume of 42,000 ft^3. The vacuum tanks are evacuated by vacuum pumps driven by a total of 500 horsepower.

As an intermittent blowdown-type tunnel, the MSFC 14-Inch TWT experiences large starting and stopping loads. This, along with the high dynamic pressures encountered through the Mach range, requires models that can stand up to these loads. It is generally assumed that the starting and stopping loads are 1.5 times the operating loads and are within the safety factor of 4 required for the wind tunnel models. The worst starting and stopping loads occur at Mach 2.74, while the highest dynamic pressure of 11 lb/in^2 is encountered at Mach 1.96. Table 3 lists the relation between Mach number, dynamic pressure, and Reynolds number per foot for the 14-Inch TWT.

TABLE 3.—*Wind tunnel operating conditions.*

Mach Number	Reynolds Number	Dynamic Pressure
0.20	1.98×10^6/ft	0.60 lb/in^2
0.30	2.8	1.30
0.60	4.7	4.36
0.80	5.5	6.47
0.90	5.9	7.36
0.95	6.2	7.76
1.05	6.1	8.48
1.10	6.2	8.76
1.15	6.2	8.99
1.25	6.2	9.31
1.46	6.0	9.49
1.96	7.2	11.00
2.74	4.7	6.38
3.48	4.8	5.15
4.96	4.4	2.73

V. TEST

A. Precursor Study

Testing was done over the Mach range of 0.3 to 5.0 at 12 selected numbers for the precursor study. These Mach numbers were 0.30, 0.60, 0.80, 0.90, 0.95, 1.05, 1.10, 1.15, 1.25, 2.74, 3.48, and 4.96. Both models were tested at angle-of-attack ranges from +6 degrees to +26 degrees at zero sideslip and at angle-of-sideslip ranges from –8 to +8 degrees at 16 degrees angle-of-attack. The reference aerodynamic axis system and reference parameters for the precursor study are shown in figure 14.

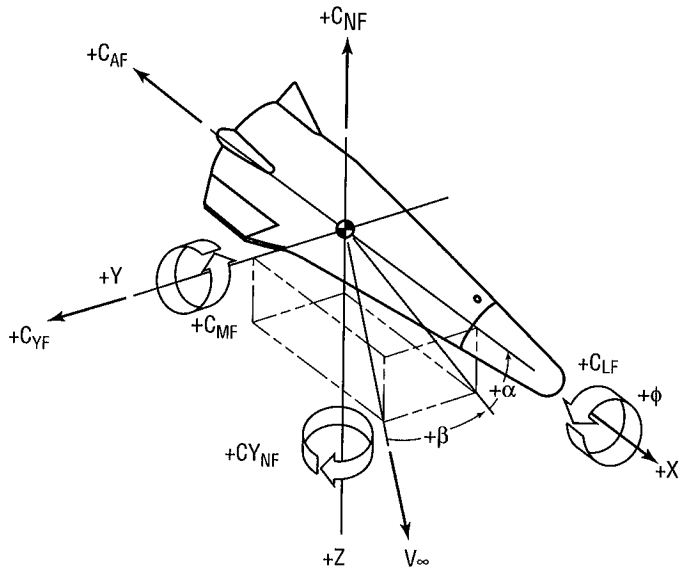

FIGURE 14.—Vertical lander aerodynamic axis system.

B. Baseline Study

A wind tunnel test over a range of Mach numbers from 0.3 to 5.0 was undertaken to determine the aerodynamic characteristics of the four models. Three of the four models were constructed using rapid prototyping methods while the fourth acted as a control, being a standard machine-tooled metal model. A wing-body-tail launch vehicle configuration was chosen to test RP processes' ability to produce accurate airfoil sections, and to determine the material property effects related to the bending of the wing and tail under loading. From a survey of past, current, and future launch vehicle concepts, it was determined that a wing-body-tail configuration was typical for the majority of configurations which would be tested. The methods of model construction were analyzed to determine the applicability of the RP processes to the design of wind tunnel models. The various RP methods were compared to determine which, if any, of these processes would be best suited to produce a wind tunnel model.

Testing was done over the Mach range of 0.3 to 5.0 at 13 selected numbers. These Mach numbers were 0.30, 0.60, 0.80, 0.90, 0.95, 1.05, 1.10, 1.15, 1.20, 1.46, 2.74, 3.48, and 4.96. All models were tested at angle-of-attack ranges from –4 degrees to +16 degrees at zero sideslip and at angle-of-sideslip ranges from –8 to +8 degrees at 6 degrees angle-of-attack. The reference aerodynamic axis system and reference parameters for the baseline study are shown in figure 15. A photograph of the stereolithography wing body model mounted in the transonic test section of the MSFC 14-Inch TWT is shown in figure 16.

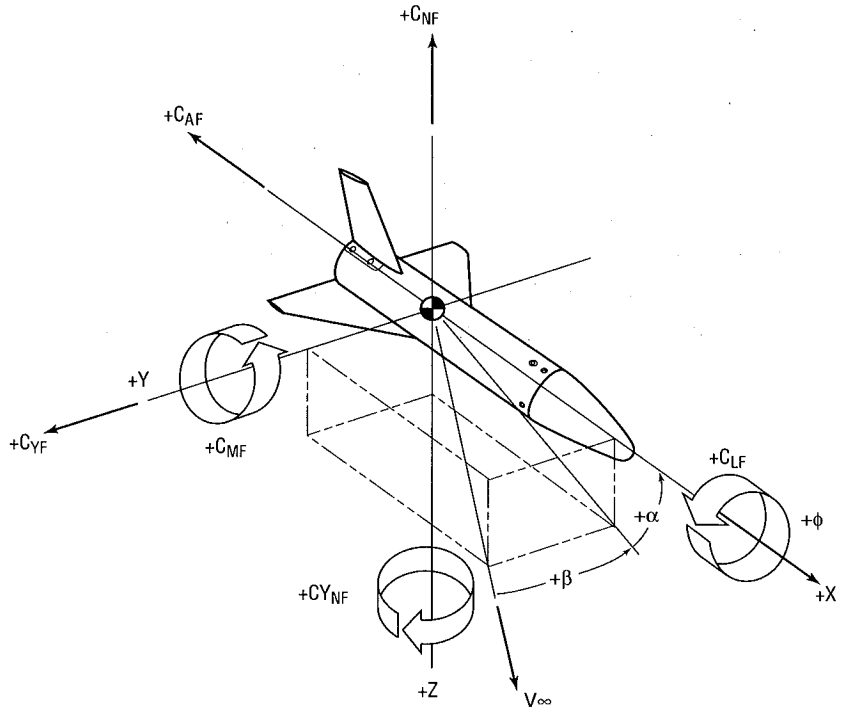

FIGURE 15.—Wing-body aerodynamic axis system.

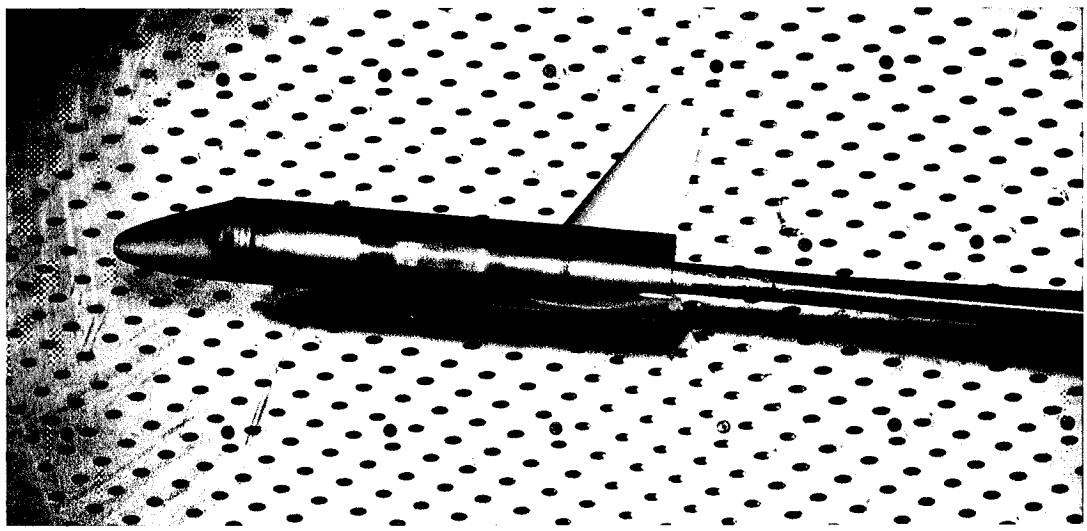

FIGURE 16.—Stereolithography model mounted in MSFC 14-Inch Trisonic Wind Tunnel transonic test section.

VI. RESULTS

A. Precursor Study

The precursor study revealed that between Mach numbers of 0.3 to 1.25, the longitudinal aerodynamic data or data in the pitch plane showed approximately a 2-degree shift in the data between the RP and metal model for the normal force (figs.17 and 20), and approximately a 1-degree data shift for the pitching moment (figs. 18 and 21). Except for these shifts, the data trends for each model type were consistent with each other. The total axial force was slightly lower for the RP model than the metal model (figs. 19 and 22). Part of the noted offset is due to the approximation for a weight tare correction. Between Mach numbers 2.74 to 4.96, only a very small shift in the data was noticed, mostly at the higher angles of attack (figs. 23 through 25). In general, it can be said that the longitudinal aerodynamic data for each model is within 5 percent. Note that no runs were made at either Mach 1.46 or 1.96 due to time constraints.

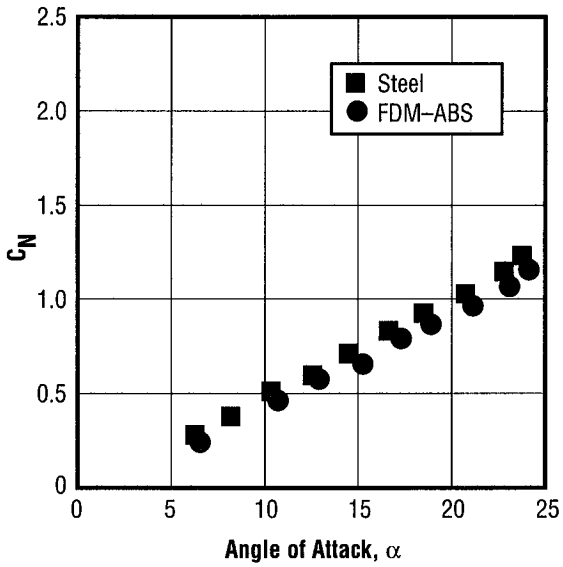

FIGURE 17.—Comparison of normal force coefficient at Mach 0.6.

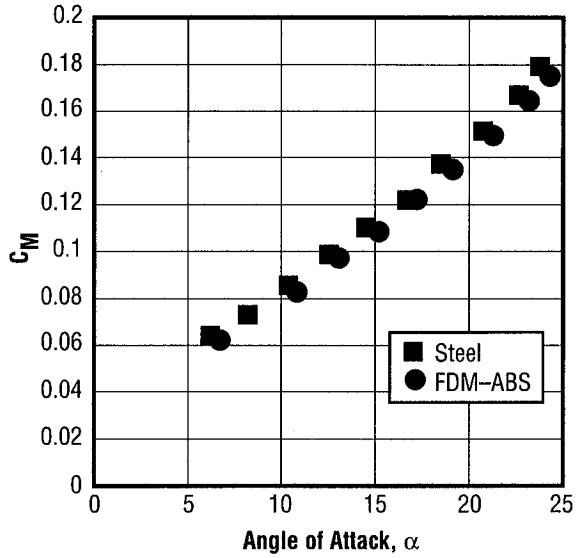

FIGURE 18.—Comparison of pitching moment coefficient at Mach 0.6.

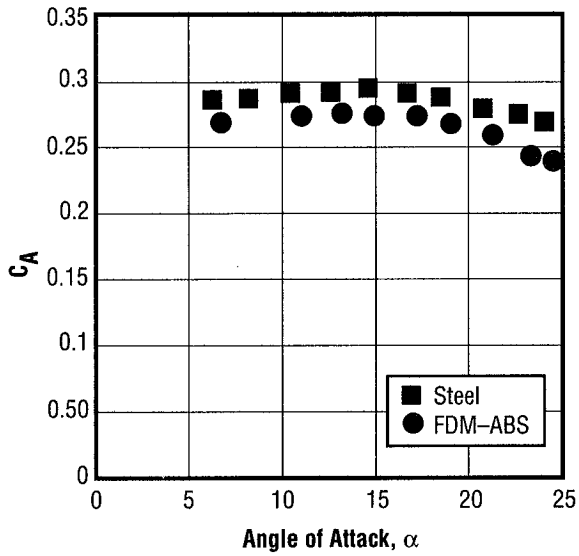

FIGURE 19.—Comparison of total axial force coefficient at Mach 0.6.

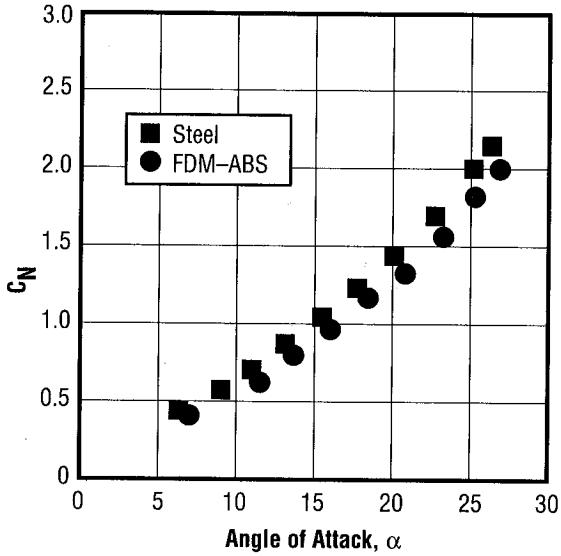

FIGURE 20.—Comparison of normal force coefficient at Mach 1.25.

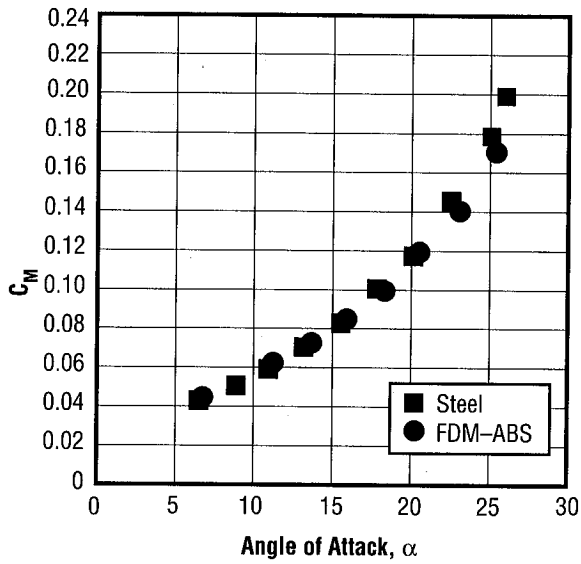

FIGURE 21.—Comparison of pitching moment coefficient at Mach 1.25.

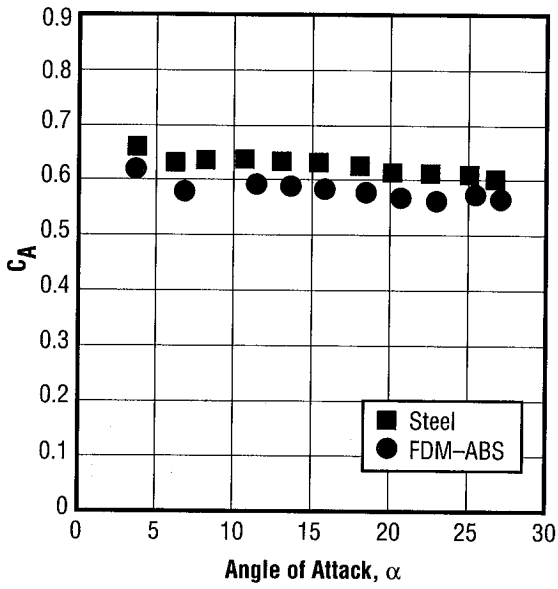

FIGURE 22.—Comparison of total axial force coefficient at Mach 1.25.

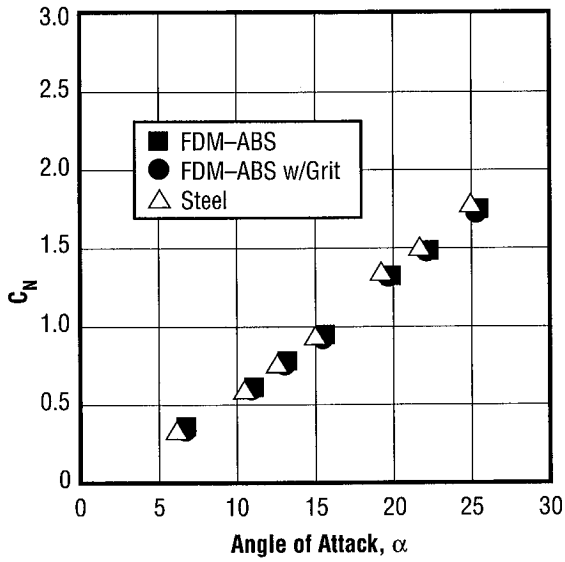

FIGURE 23.—Comparison of normal force coefficient at Mach 2.74.

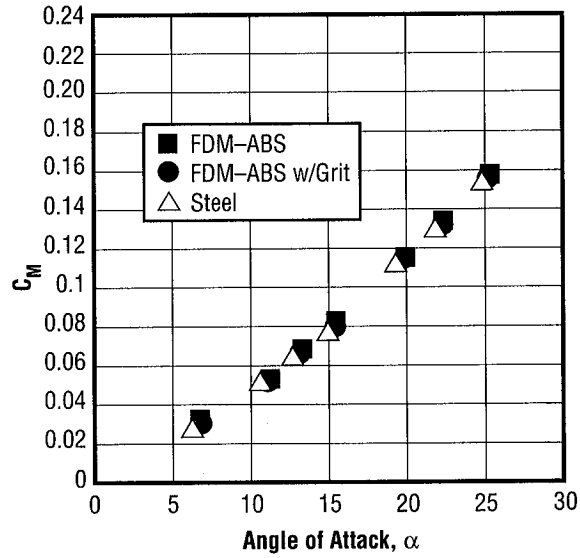

FIGURE 24.—Comparison of pitching moment coefficient at Mach 2.74.

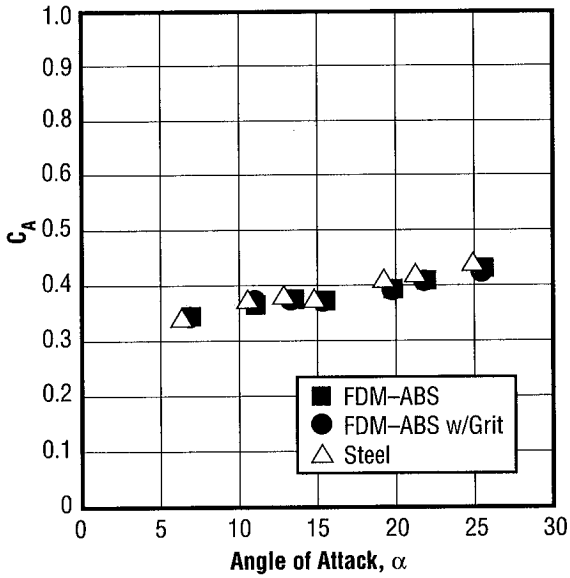

FIGURE 25.—Comparison of total axial force coefficient at Mach 2.74.

The lateral directional aerodynamic data show some small discrepancies between the two model types. Since the vehicle is symmetric in the X–Y plane (i.e., the port side is the same as the starboard side) the lateral aerodynamic data should go through zero at zero degrees sideslip angle. Subsonically and transonically both sets of data show slight zero offset shifts, with the RP model showing a larger shift than the metal model (figs. 26 through 34). These zero shifts in the data were caused by an unexpected error in roll during the installation of the balance adapters in the models. The metal model having approximately a 0.2-degree roll, and the RP model approximately a 2.5-degree roll in the balance adapter installation. The data do, however, show a slight shift in the data trends between the models. On average, there is a .003 shift in the side force data trends slope and a .0002 shift in the yawing moment data trends slope between the metal and the RP models as shown in figures 26, 29, 32, and 27, 30, 33. Representative Mach numbers of 0.6, 1.25, and 2.74 have been used to display the data trends.

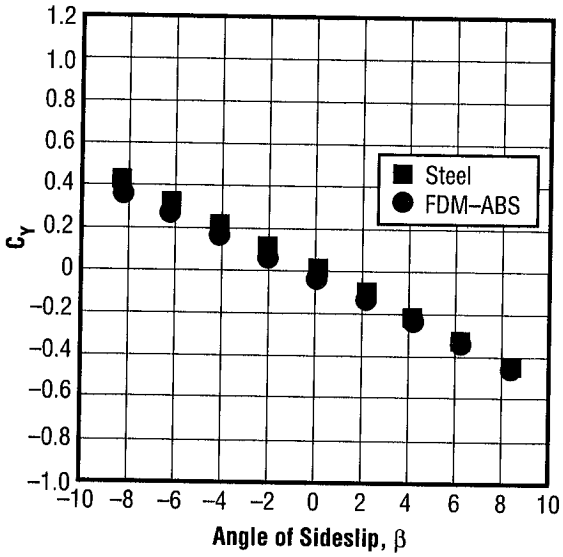

FIGURE 26.—Comparison of side force coefficient at Mach 0.6.

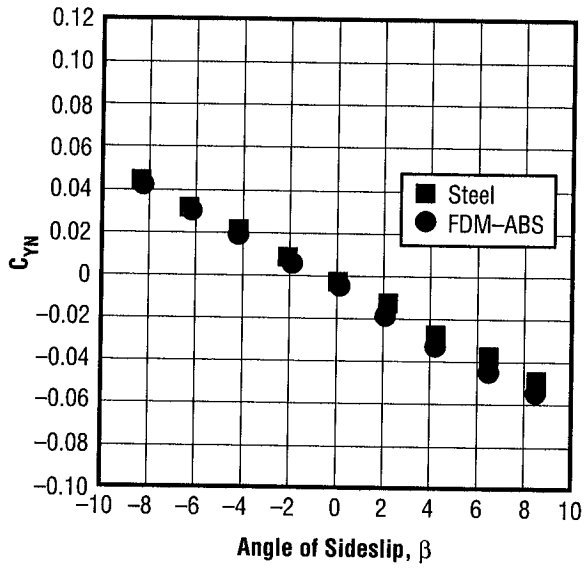

FIGURE 27.—Comparison of yawing moment coefficient at Mach 0.6.

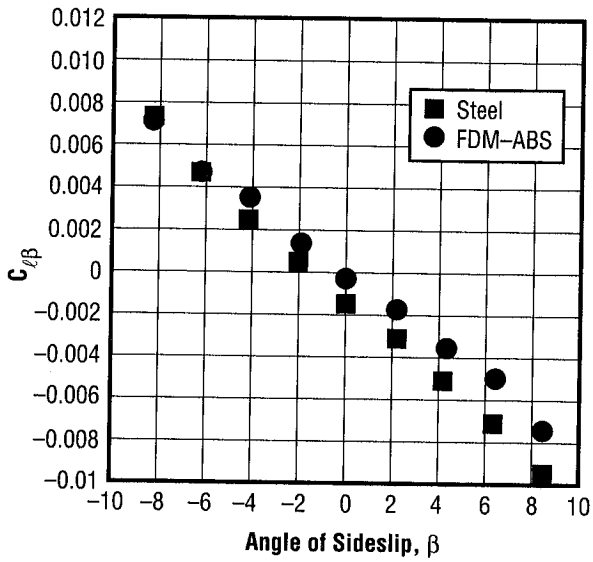

FIGURE 28.—Comparison of rolling side moment coefficient at Mach 0.6.

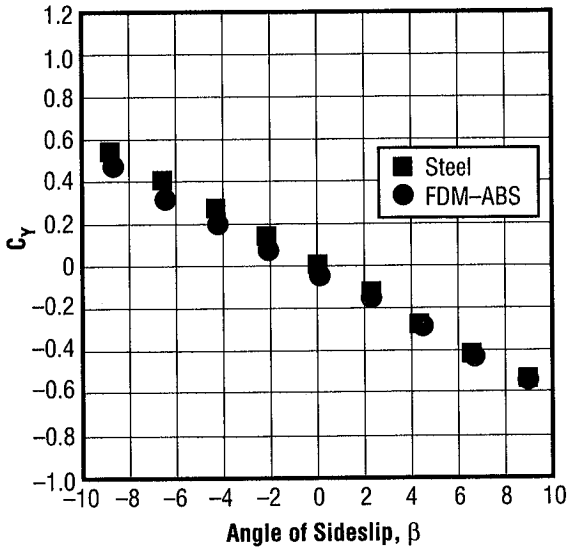

FIGURE 29.—Comparison of side force coefficient at Mach 1.25.

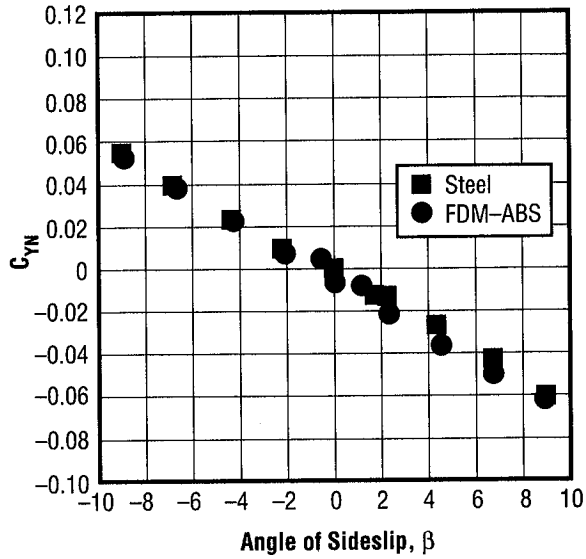

FIGURE 30.—Comparison of yawing moment coefficient at Mach 1.25.

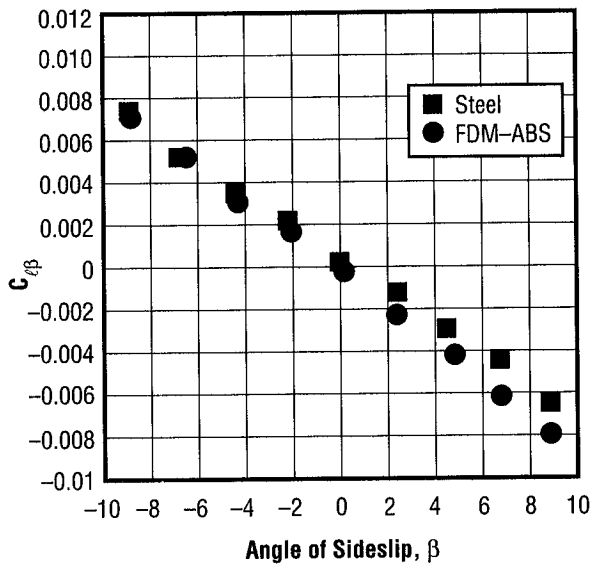

FIGURE 31.—Comparison of rolling side moment coefficient at Mach 1.25.

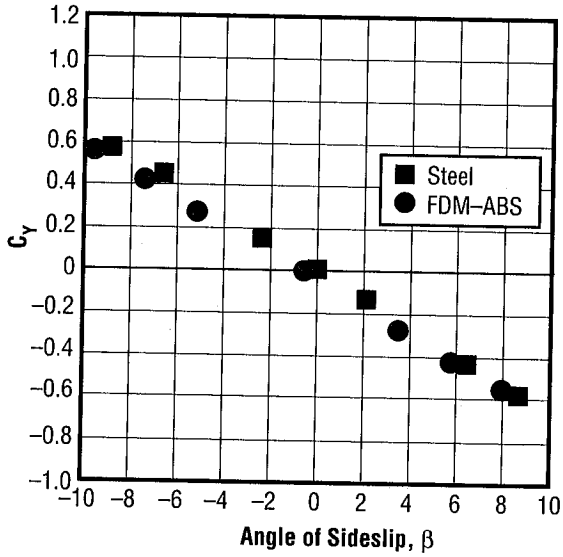

FIGURE 32.—Comparison of side force coefficient at Mach 2.74.

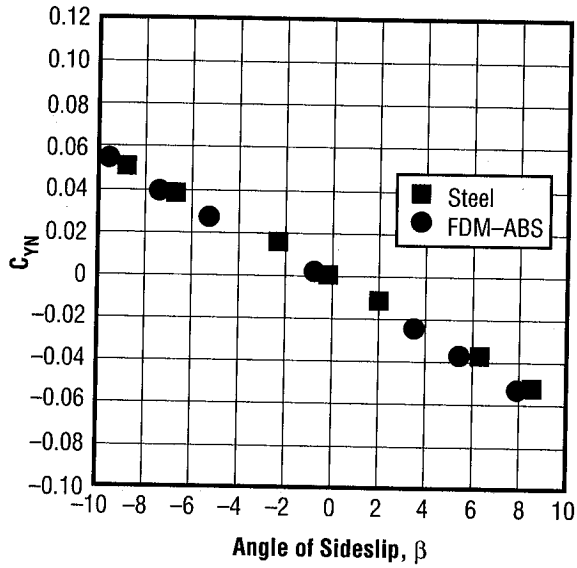

FIGURE 33.—Comparison of yawing moment coefficient at Mach 2.74.

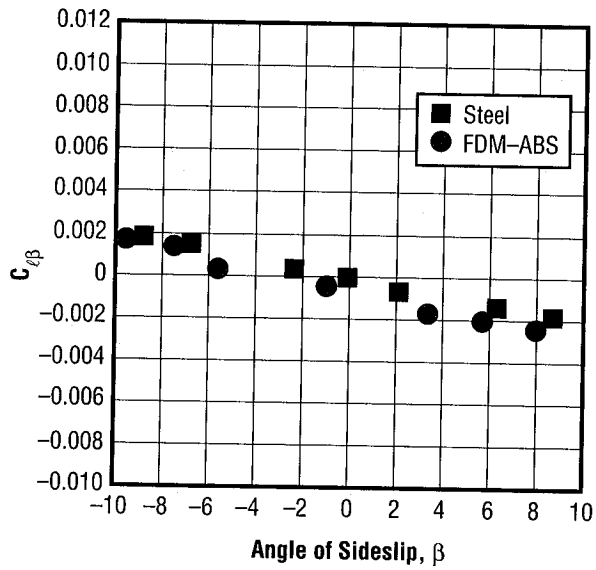

FIGURE 34.—Comparison of rolling side moment coefficient at Mach 2.74.

B. Baseline Study

For all phases of the baseline study representative Mach numbers of 0.3, 0.8, 1.05, 1.2, 3.48, and 4.96 are presented in this report. Coefficients of normal force, axial force, pitching moment, and lift over drag are shown at each of these Mach numbers. Only longitudinal data are shown for this study.

1. Baseline Models

The study showed that between Mach numbers of 0.3 to 1.2, the longitudinal aerodynamic data or data in the pitch plane showed very good agreement between the metal model and SLA model up to about 12 degrees angle-of-attack when it started to diverge due to assumed SLA model surface bending under higher loading (figs. 35 through 50). The initial SLS data for all the coefficients do not accurately represent the process because the model was a different configuration due to post-processing problems. The second SLS model tested showed much better agreement with the data trends from the other models, but was not as good as the FDM and SLA. The greatest difference in the aerodynamic data between the models at Mach numbers of 0.3 to 1.2 was in total axial force. Between Mach numbers of 2.74 to 4.96 all the models showed good agreement in axial force (figs. 51 through 58). In general, it can be said that all the RP model longitudinal aerodynamic data at subsonic Mach numbers showed a slight divergence at higher angles-of-attack when compared to the metal model data. At transonic Mach numbers the majority of the configurations started diverging at about 10 to 12 degrees angle-of-attack due to the higher loads encountered by the models. Finally, at the supersonic Mach numbers, the data showed good agreement over the angle-of-attack range tested. These data are shown in figures 35 through 58.

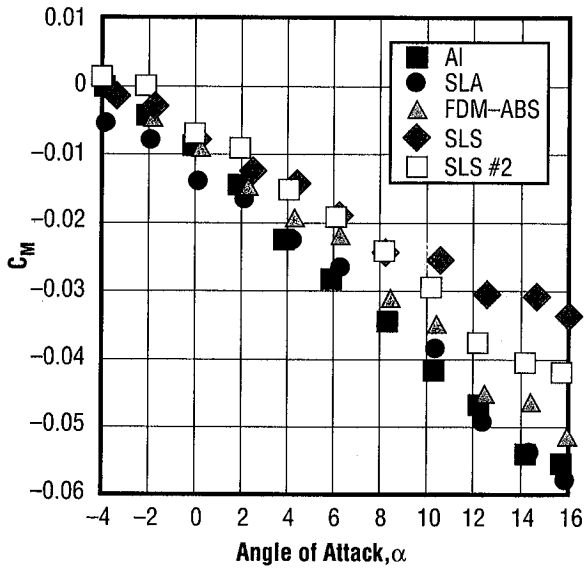

FIGURE 35.—Comparison of pitching moment coefficient at Mach 0.3.

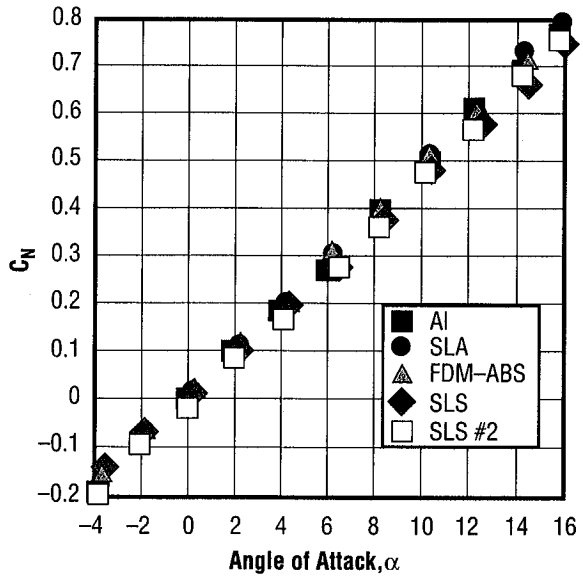

FIGURE 36.—Comparison of normal force coefficient at Mach 0.3.

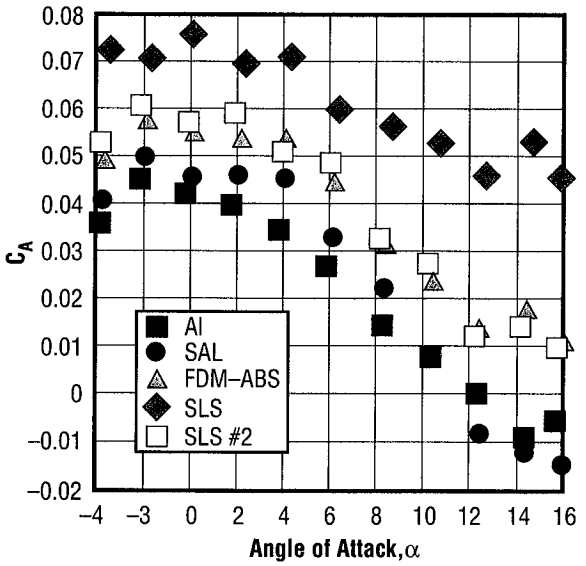

FIGURE 37.—Comparison of axial force coefficient at Mach 0.3.

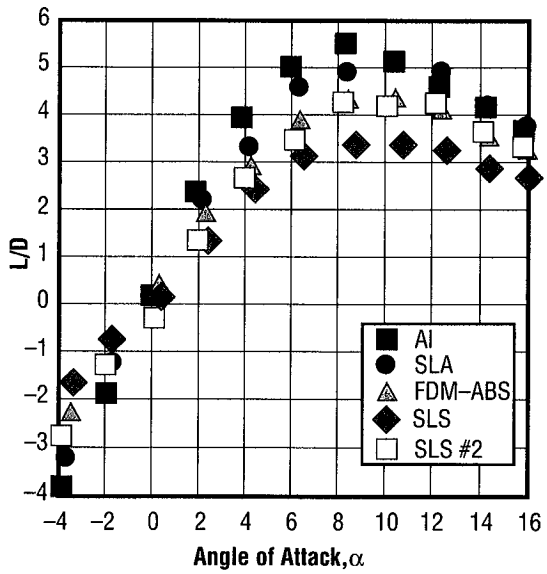

FIGURE 38.—Comparison of lift over drag at Mach 0.3.

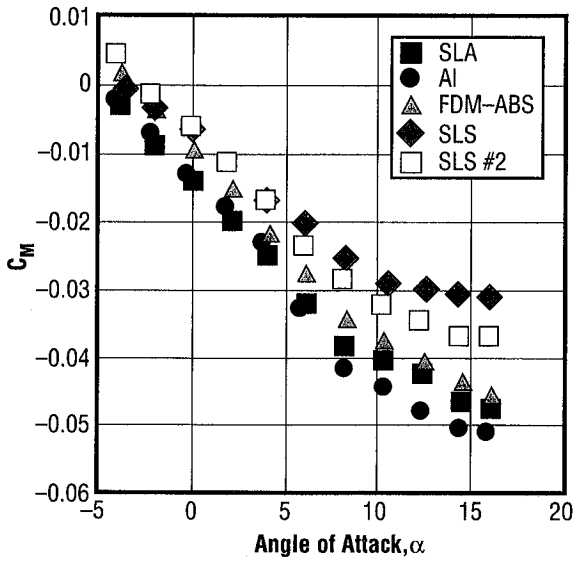

FIGURE 39.—Comparison of pitching moment coefficient at Mach 0.8.

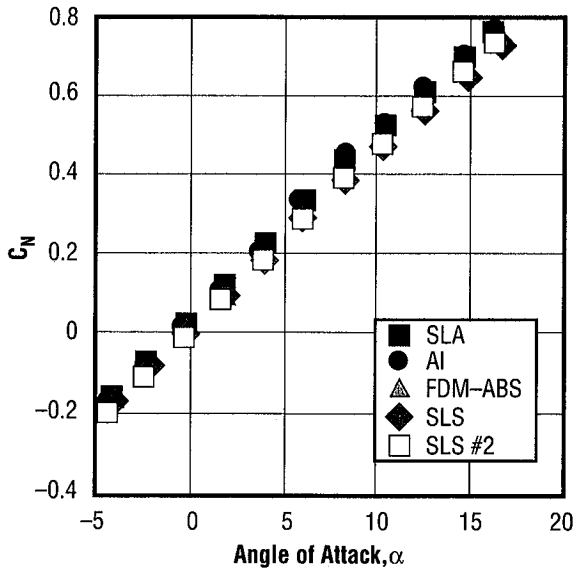

FIGURE 40.—Comparison of normal force coefficient at Mach 0.8.

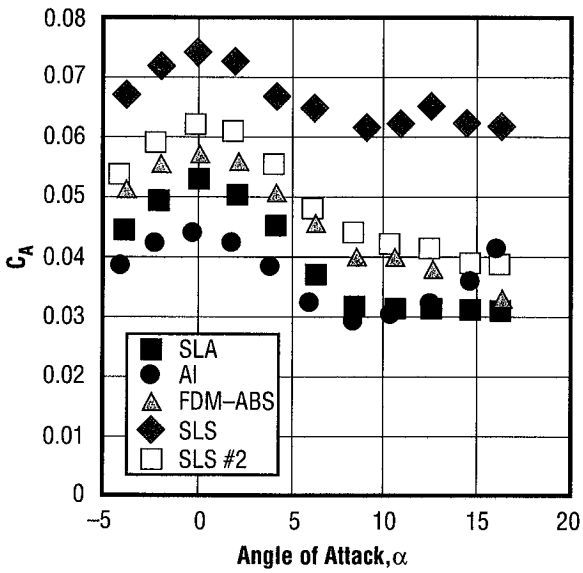

FIGURE 41.—Comparison of axial force coefficient at Mach 0.8.

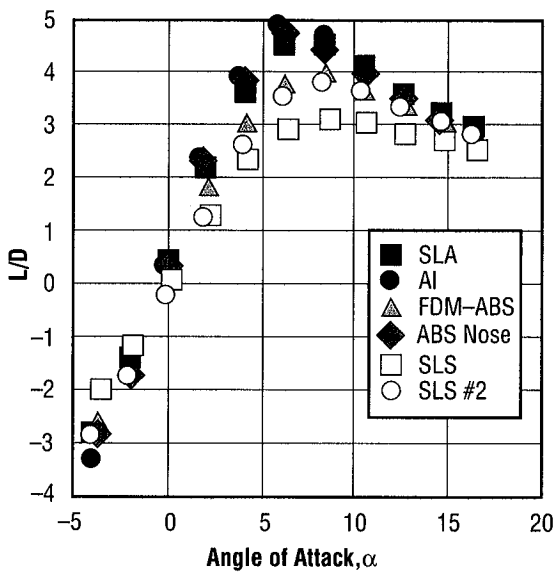

FIGURE 42.—Comparison of lift over drag at Mach 0.8.

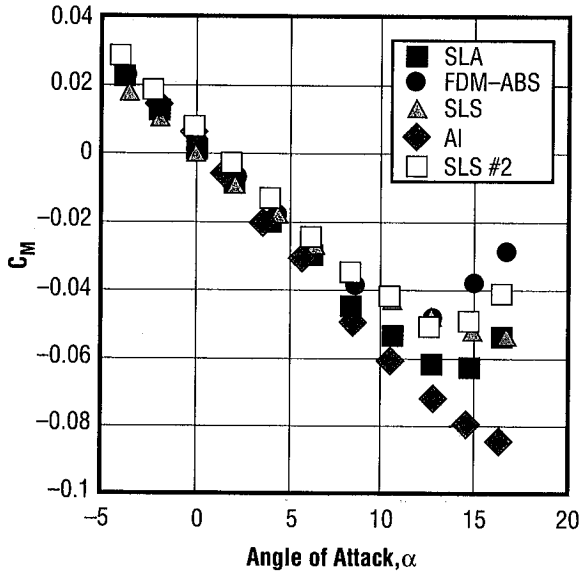

FIGURE 43.—Comparison of pitching moment coefficient at Mach 1.05.

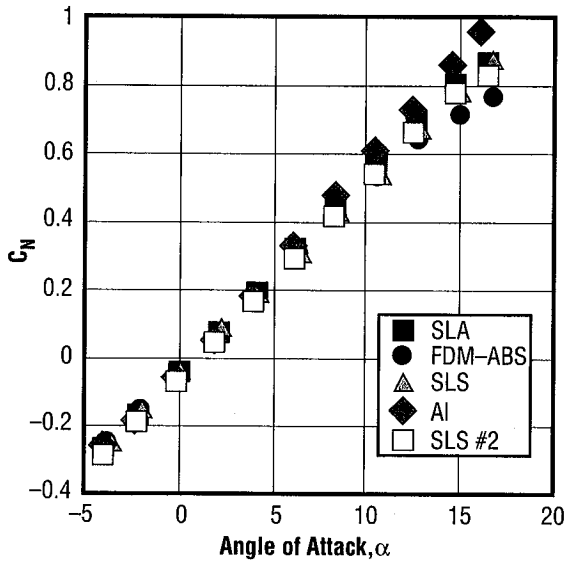

FIGURE 44.—Comparison of normal force coefficient at Mach 1.05.

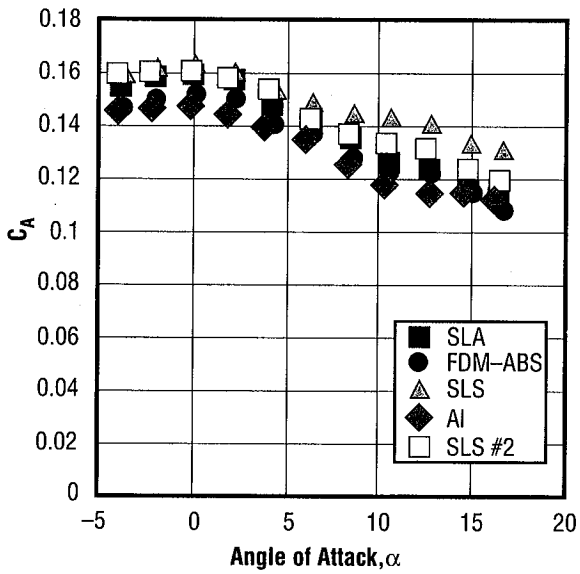

FIGURE 45.—Comparison of axial force coefficient at Mach 1.05.

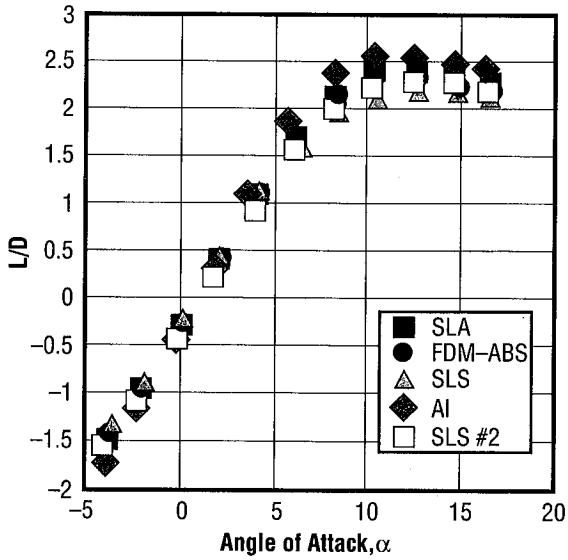

FIGURE 46.—Comparison of lift over drag at Mach 1.05.

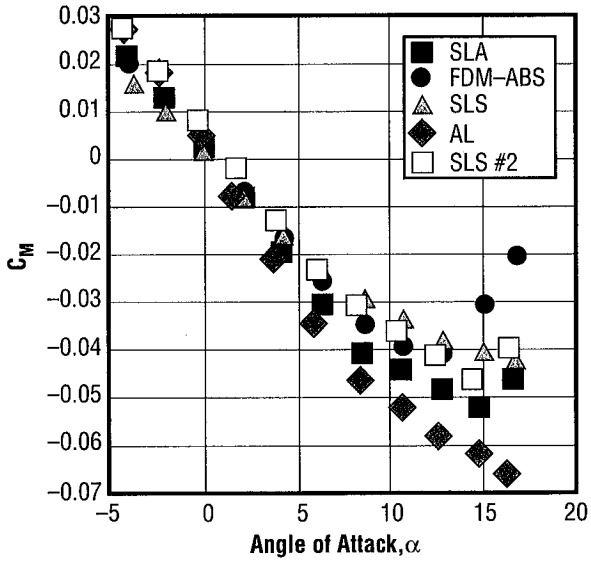

FIGURE 47.—Comparison of pitching moment coefficient at Mach 1.2.

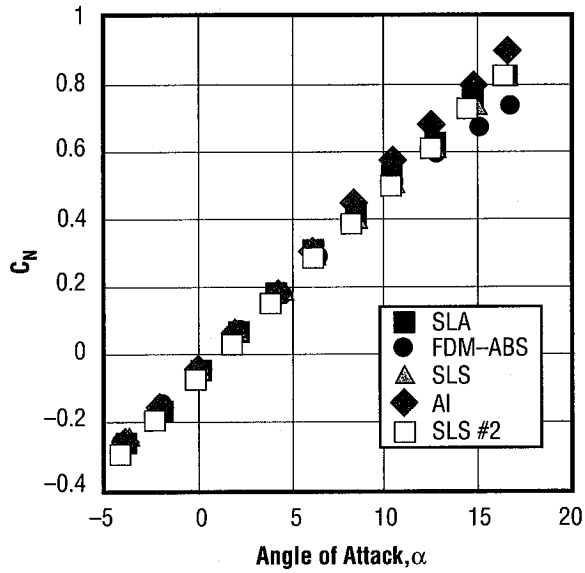

FIGURE 48.—Comparison of normal force coefficient at Mach 1.2.

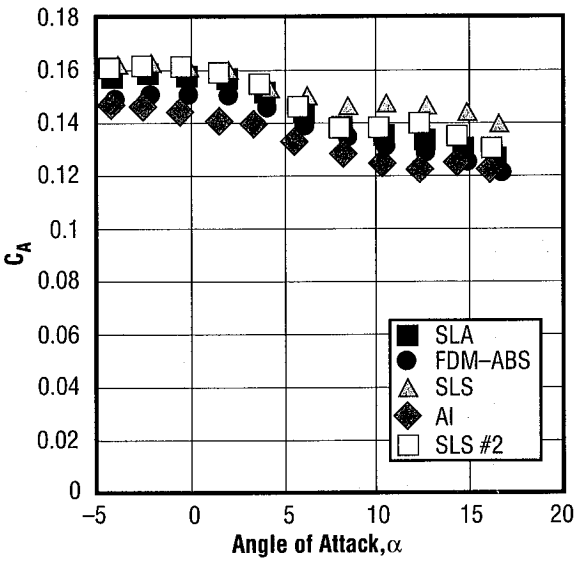

FIGURE 49.—Comparison of axial force coefficient at Mach 1.2.

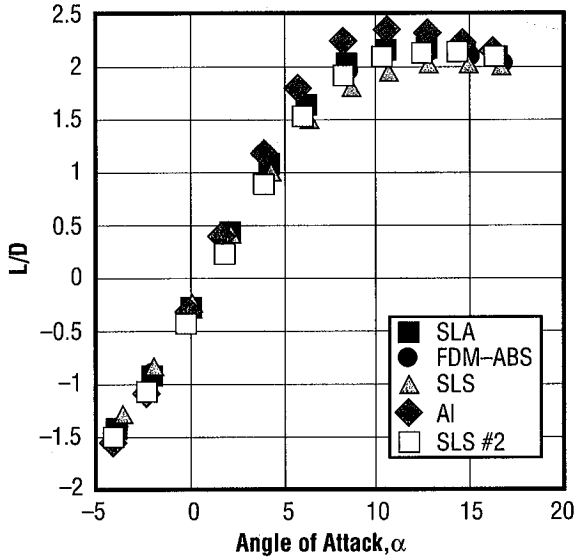

FIGURE 50.—Comparison of lift over drag at Mach 1.2.

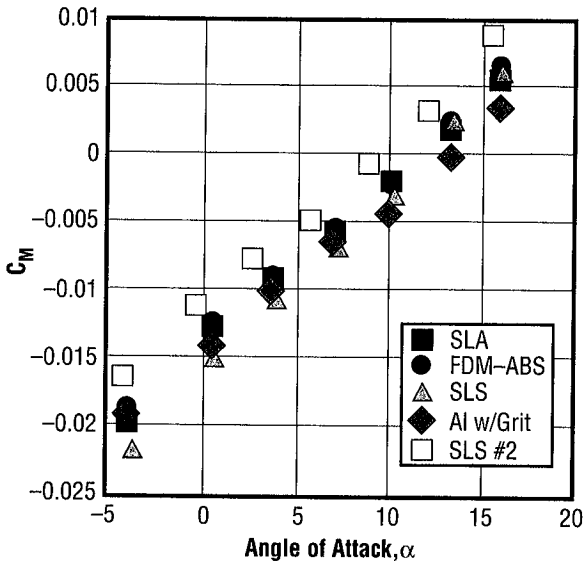

FIGURE 51.—Comparison of pitching moment coefficient at Mach 3.48.

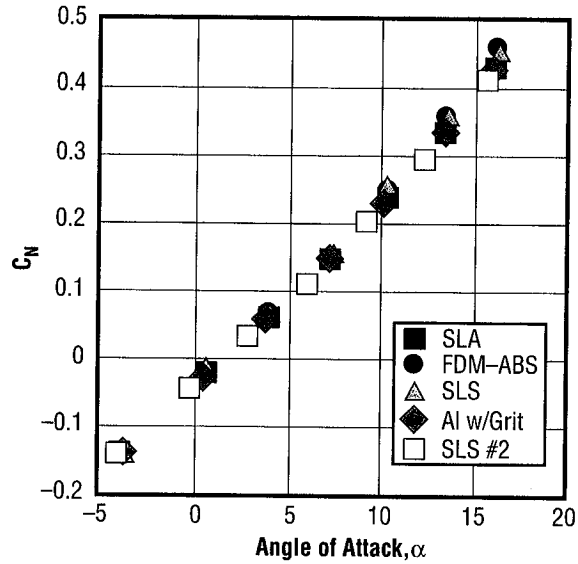

FIGURE 52.—Comparison of normal force coefficient at Mach 3.48.

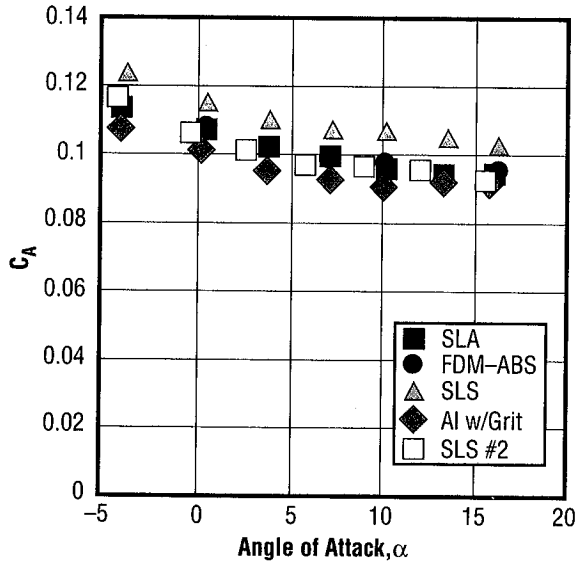

FIGURE 53.—Comparison of axial force coefficient at Mach 3.48.

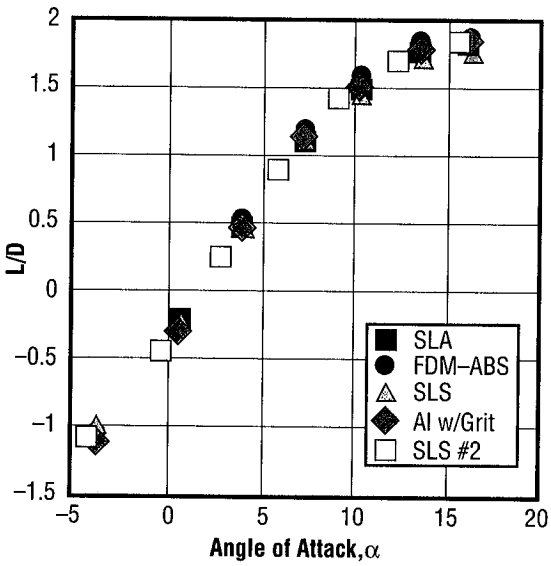

FIGURE 54.—Comparison of lift over drag at Mach 3.48.

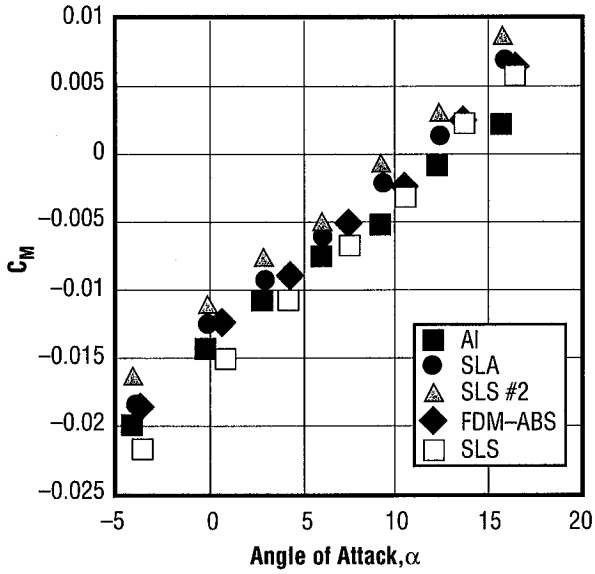

FIGURE 55.—Comparison of pitching moment coefficient at Mach 4.96.

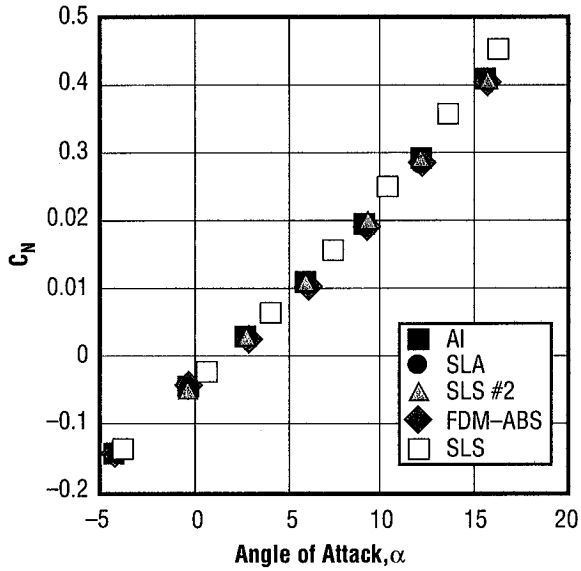

FIGURE 56.—Comparison of normal force coefficient at Mach 4.96.

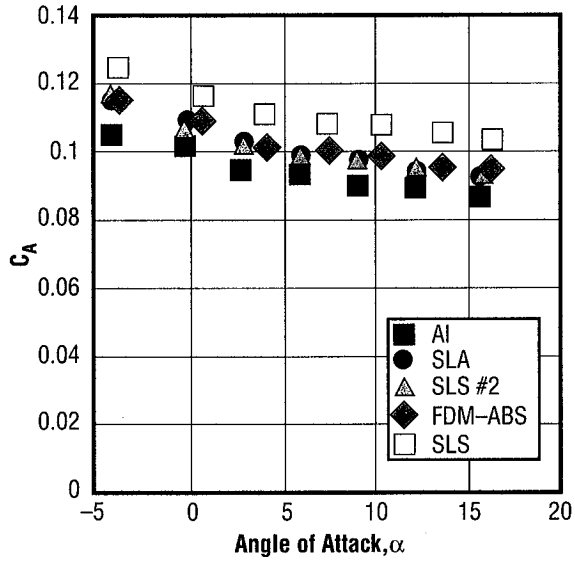

FIGURE 57.—Comparison of axial force coefficient at Mach 4.96.

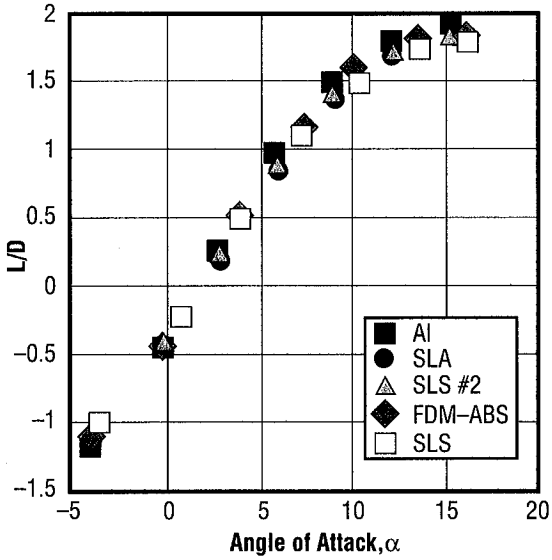

FIGURE 58.—Comparison of lift over drag at Mach 4.96.

2. Replacement Parts

Along with the baseline study, the replacement of standard machined metal model parts with those of RP parts was undertaken. The study showed that between Mach numbers of 0.3 to 1.2, the longitudinal aerodynamic data showed very good agreement between the metal model and the metal model with the replacement FDM–ABS nose and SLA nose. The supersonic data showed a slight divergence between the data but the data trends were consistent. The data from the replacement part phase of the test is plotted in figures 59 through 82. The aluminum model with the FDM–ABS and SLA replacement noses is shown in figure 83.

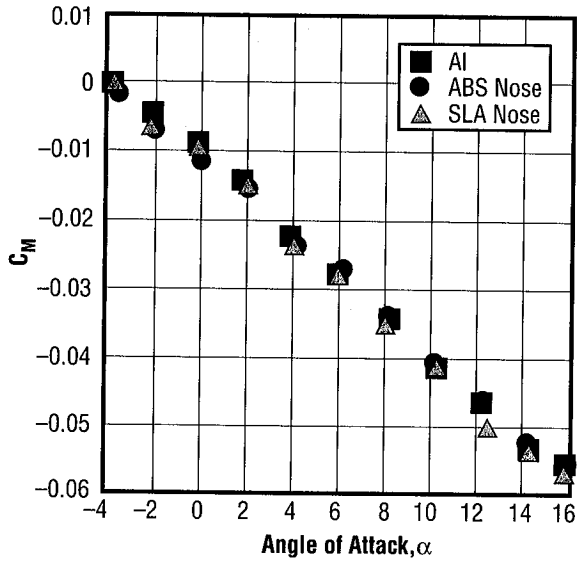

FIGURE 59.—Comparison of pitching moment coefficient at Mach 0.3.

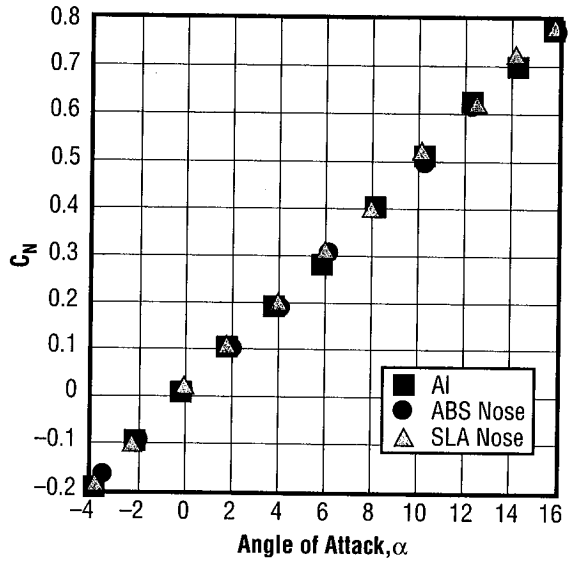

FIGURE 60.—Comparison of normal force coefficient at Mach 0.3.

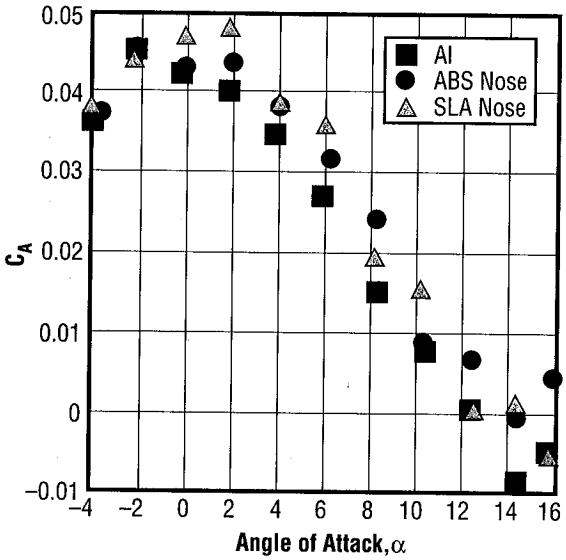

FIGURE 61.—Comparison of axial force coefficient at Mach 0.3.

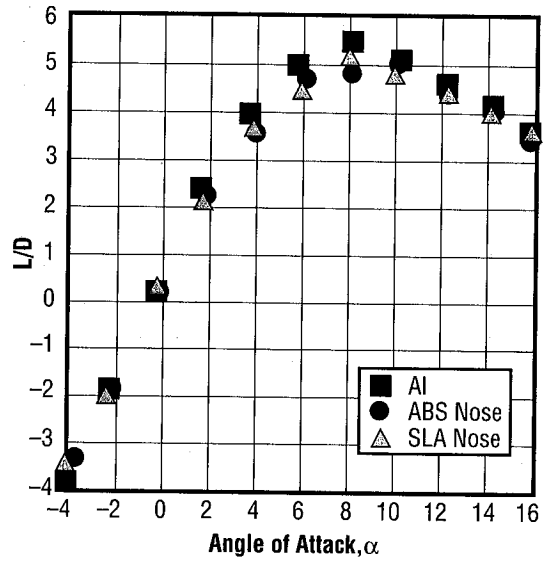

FIGURE 62.—Comparison of lift over drag at Mach 0.3.

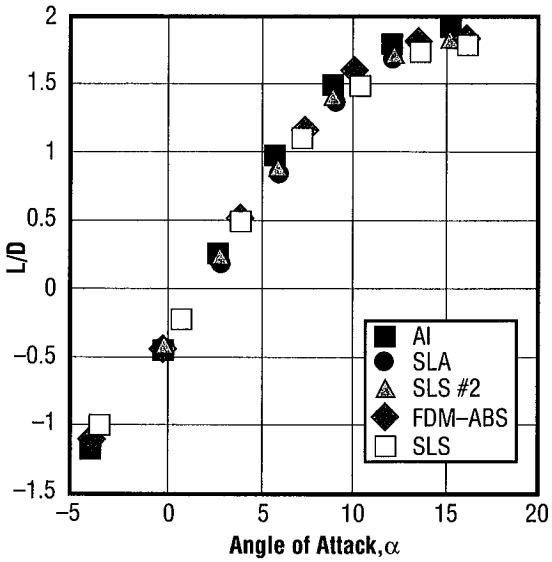

FIGURE 63.—Comparison of pitching moment coefficient at Mach 0.8.

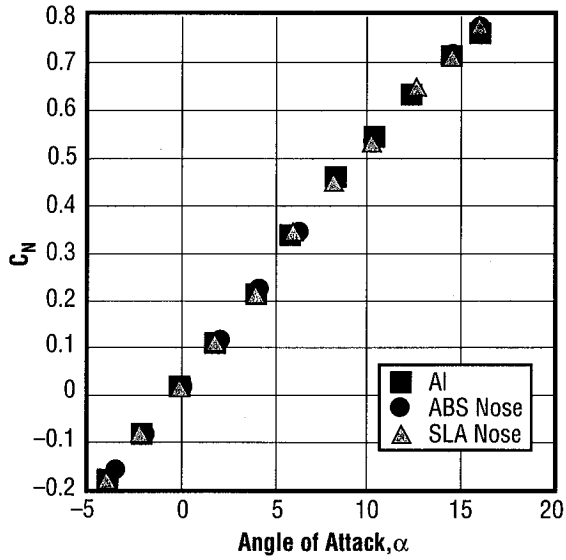

FIGURE 64.—Comparison of normal force coefficient at Mach 0.8.

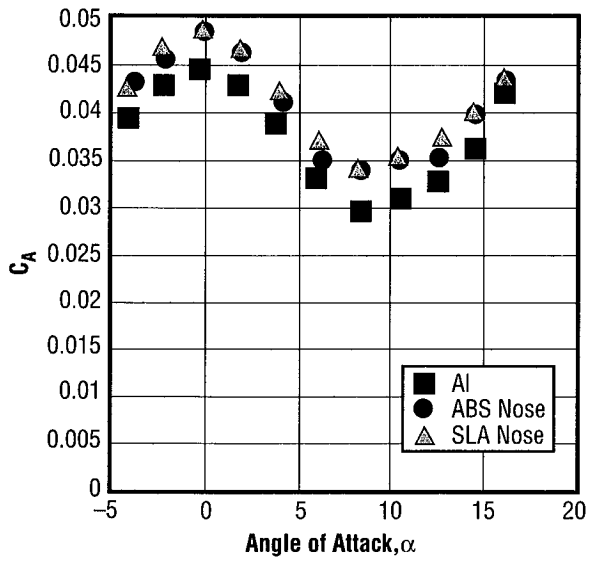

FIGURE 65.—Comparison of axial force coefficient Mach 0.8.

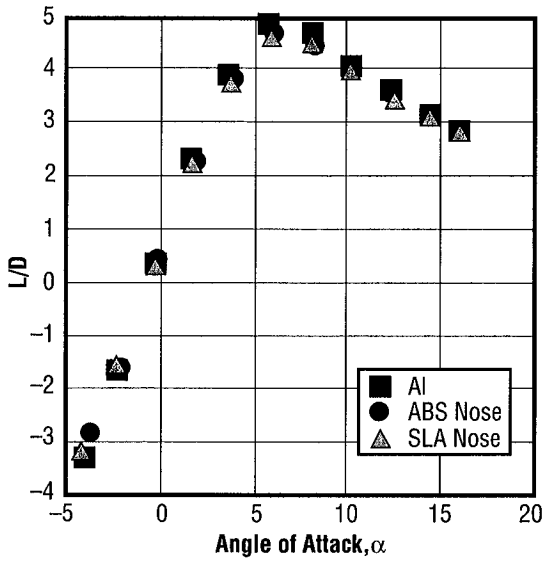

FIGURE 66.—Comparison of lift over drag at Mach 0.8.

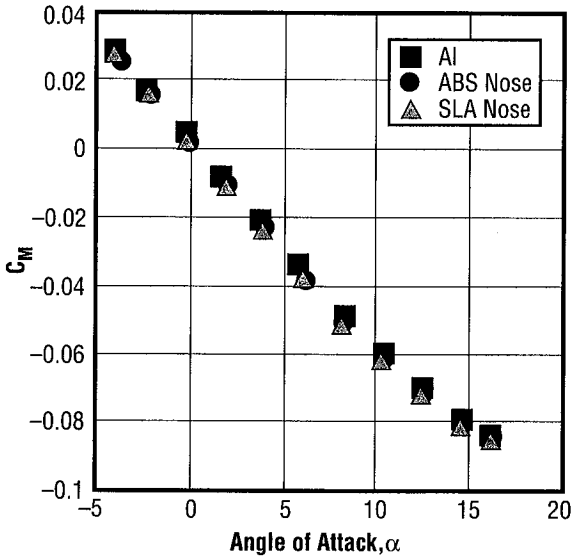

FIGURE 67.—Comparison of pitching moment coefficient at Mach 1.05.

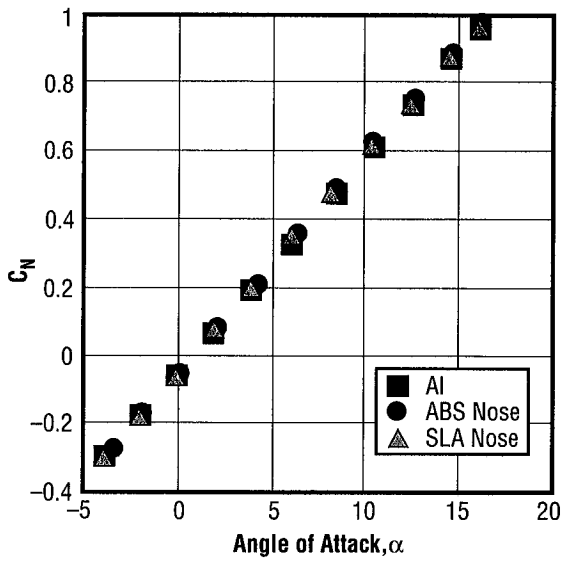

FIGURE 68.—Comparison of normal force coefficient at Mach 1.05.

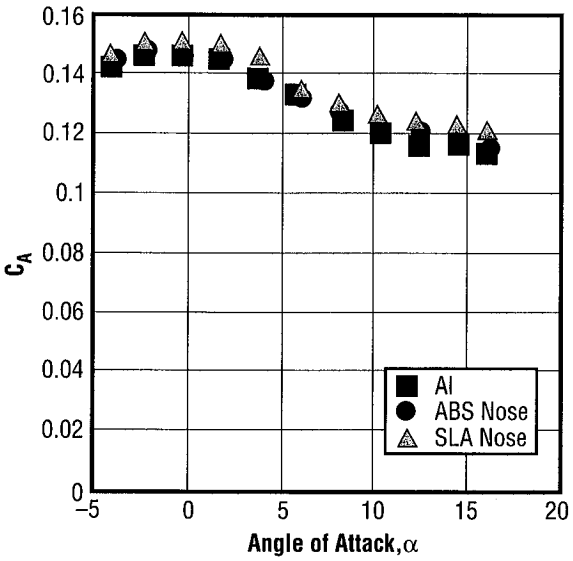

FIGURE 69.—Comparison of axial force coefficient at Mach 1.05.

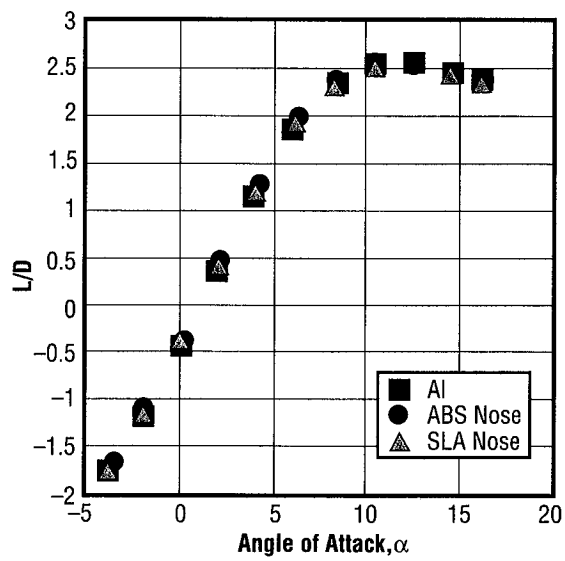

FIGURE 70.—Comparison of lift over drag at Mach 1.05.

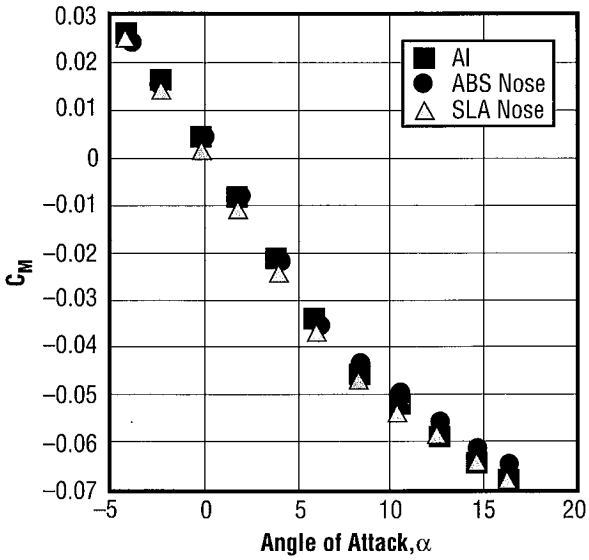

FIGURE 71.—Comparison of pitching moment coefficient at Mach 1.2.

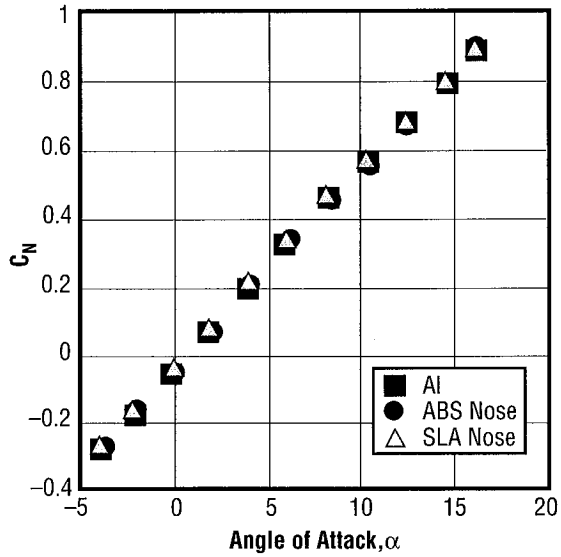

FIGURE 72.—Comparison of normal force coefficient at Mach 1.2.

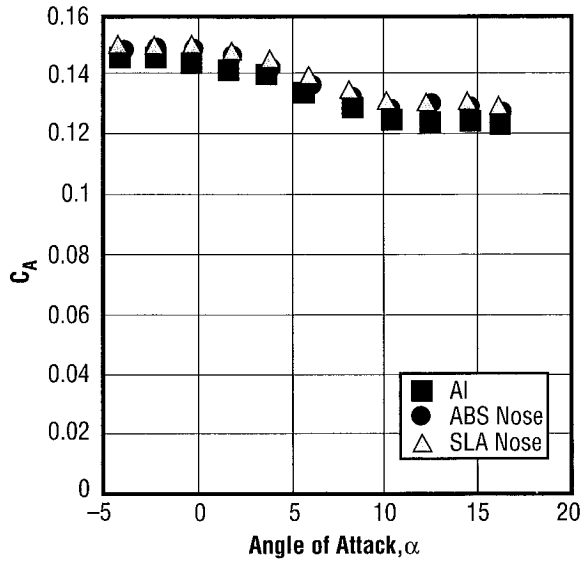

FIGURE 73.—Comparison of axial force coefficient at Mach 1.2.

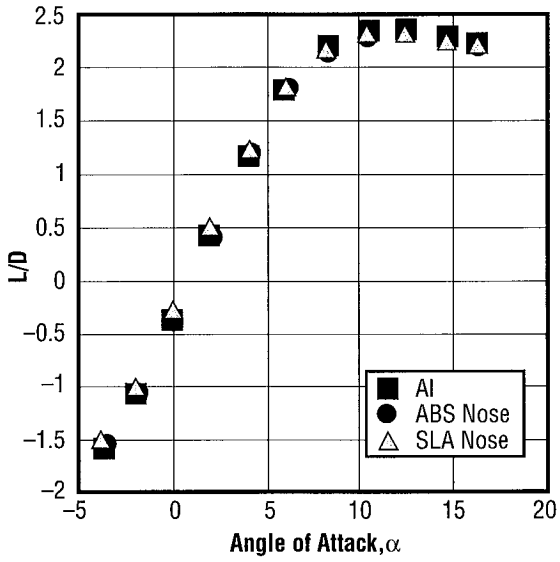

FIGURE 74.—Comparison of lift over drag at Mach 1.2.

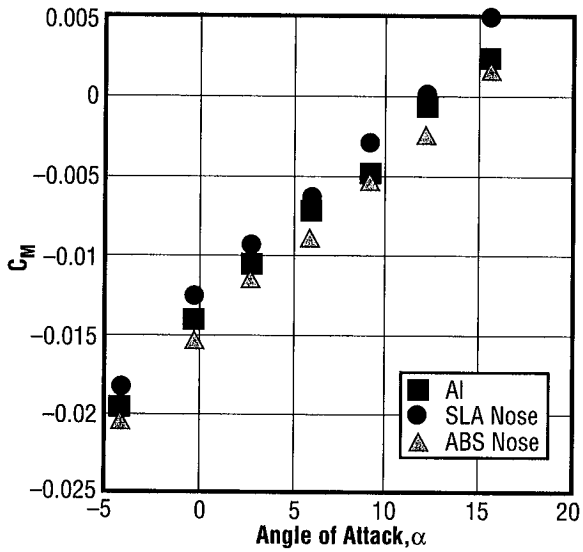

FIGURE 75.—Comparison of pitching moment coefficient at Mach 3.48.

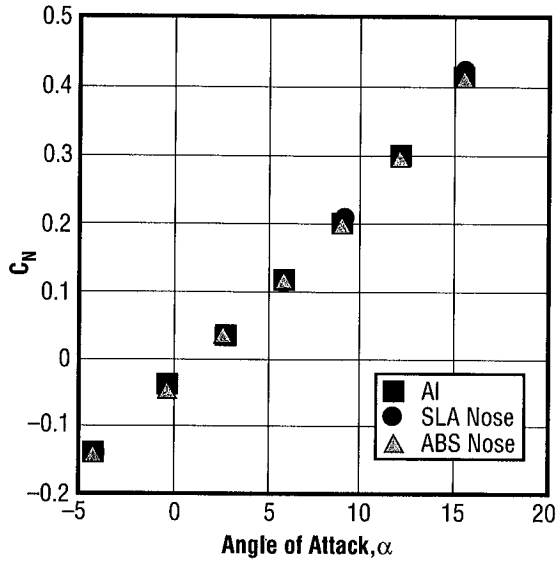

FIGURE 76.—Comparison of normal force coefficient at Mach 3.48.

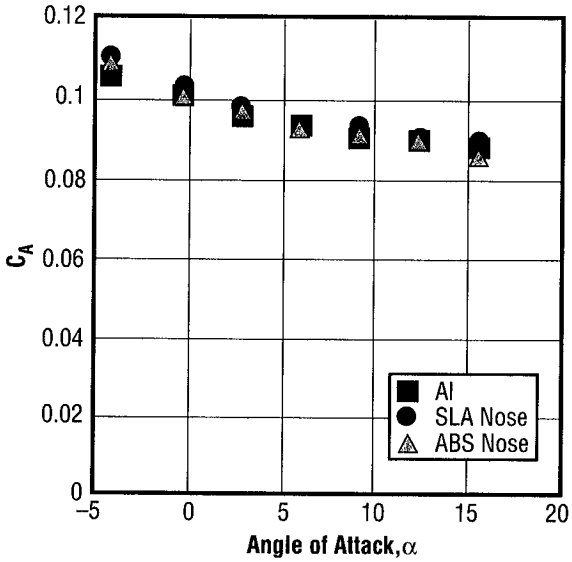

FIGURE 77.—Comparison of axial force coefficient at Mach 3.48.

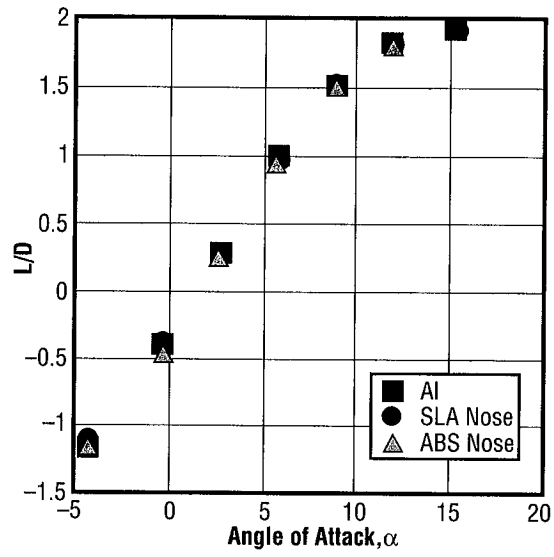

FIGURE 78.—Comparison of lift over drag at Mach 3.48.

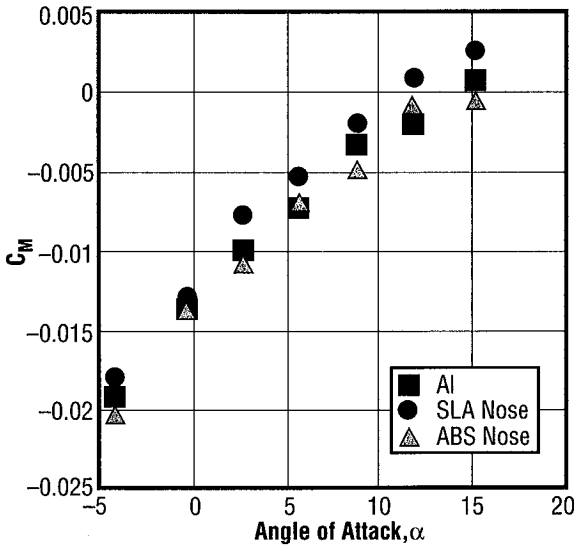

FIGURE 79.—Comparison of pitching moment coefficient at Mach 4.96.

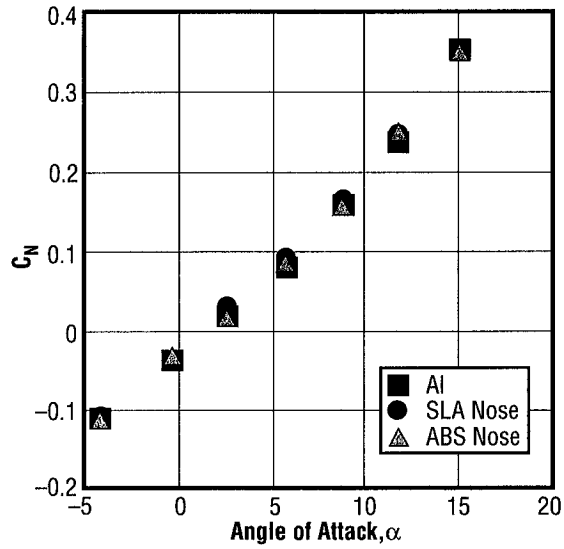

FIGURE 80.—Comparison of normal force coefficient at Mach 4.96.

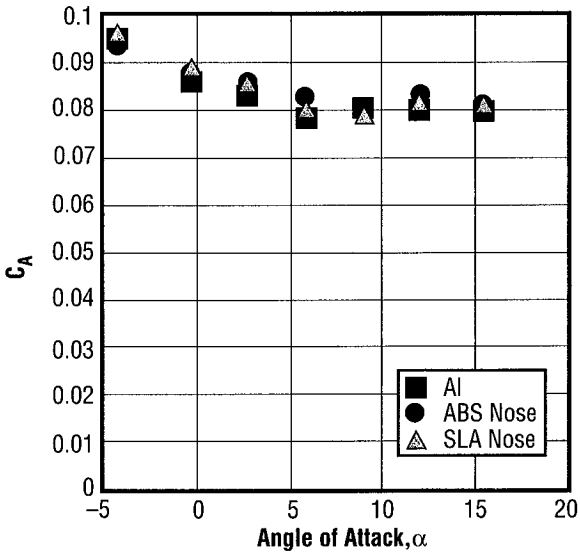

FIGURE 81.—Comparison of axial force coefficient at Mach 4.96.

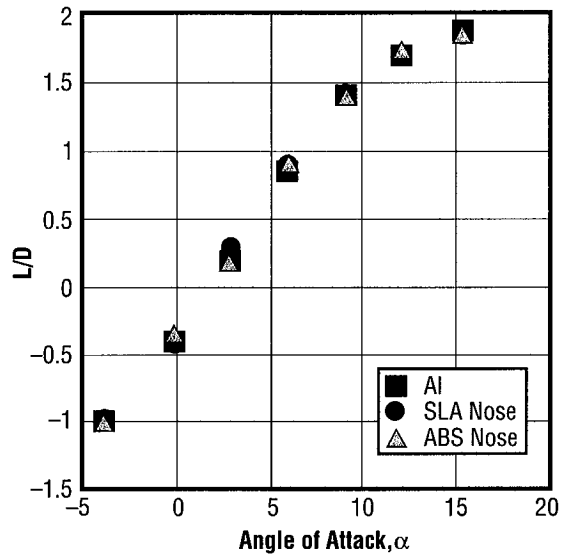

FIGURE 82.—Comparison of lift over drag at Mach 4.96.

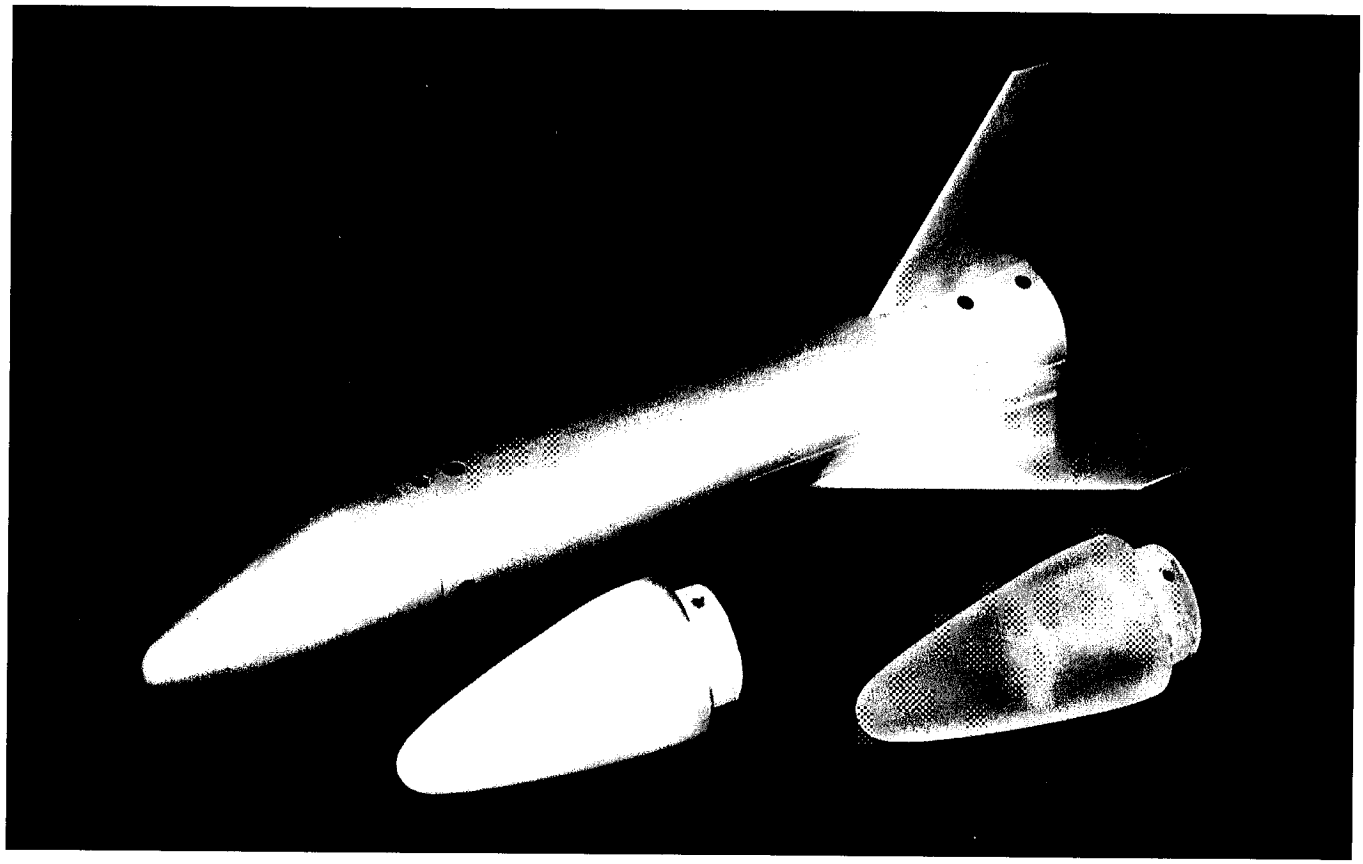

FIGURE 83.—Aluminum wing-body model with fused deposition and stereolithography replacement noses.

3. Surface Finish

The effects of surface finish and grit on the aerodynamic characteristics of the models were determined. The RP models did not have as smooth a finish as did the aluminum model, so runs were made to determine if the difference in these surface finishes would affect the aerodynamic characteristics. A rough surface finish was simulated on the aluminum model by covering the full model in a layer of silicon carbide particles called "grit." This grit would "rough" up the surface. The effect of grit on the model was also determined. Grit is used to trip the boundary layer over the model to simulate a higher Reynolds number than the actual wind tunnel Reynolds number. Number 100 silicon carbide particles, or grit, were applied in a ring around the nose and on the upper and lower surfaces 0.1-inch aft of the leading wing edge. Number 100 grit has a nominal spherical particle diameter of 0.0059 inch. The effect of these changes is shown in figures 84 through 107. In these graphs it can be seen that surface finish does have an effect on the aerodynamic characteristics up to supersonic speeds where the effect is less drastic than at lower Mach numbers. The application of grit had little effect on the aerodynamic characteristics except for axial force and its derivative coefficients.

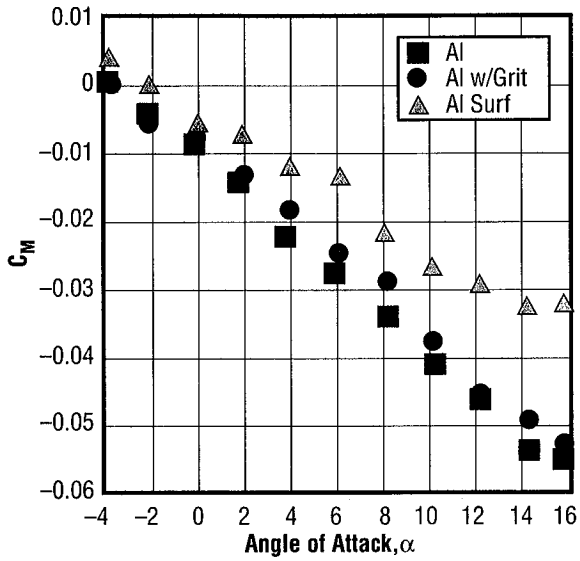

FIGURE 84.—Comparison of pitching moment coefficient at Mach 0.3.

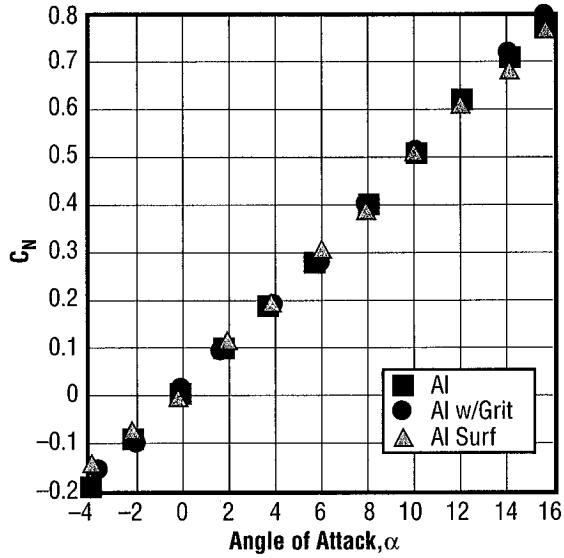

FIGURE 85.—Comparison of normal force coefficient at Mach 0.3.

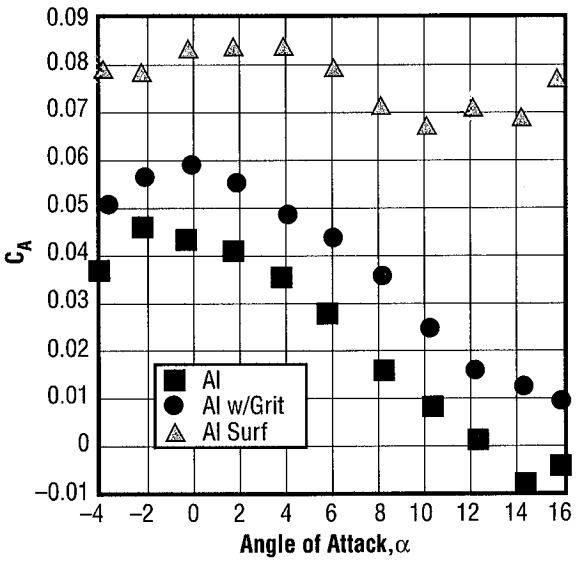

FIGURE 86.—Comparison of axial force coefficient at Mach 0.3.

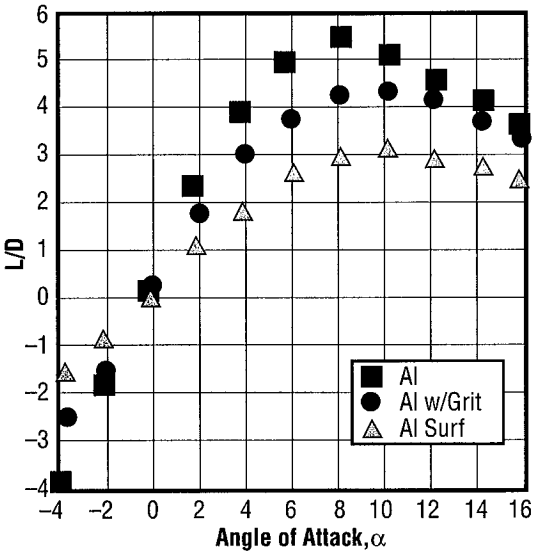

FIGURE 87.—Comparison of lift over drag at Mach 0.3.

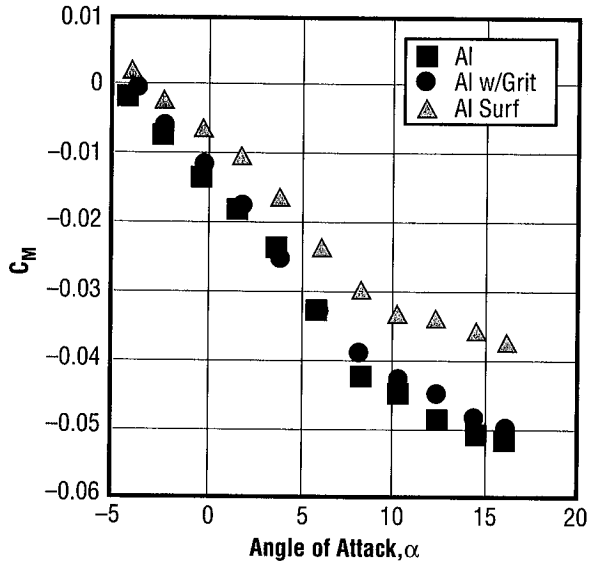

FIGURE 88.—Comparison of pitching moment coefficient at Mach 0.8.

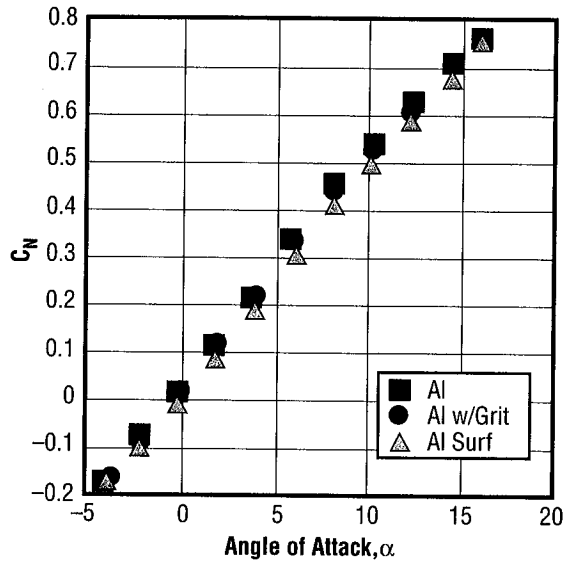

FIGURE 89.—Comparison of normal force coefficient at Mach 0.8.

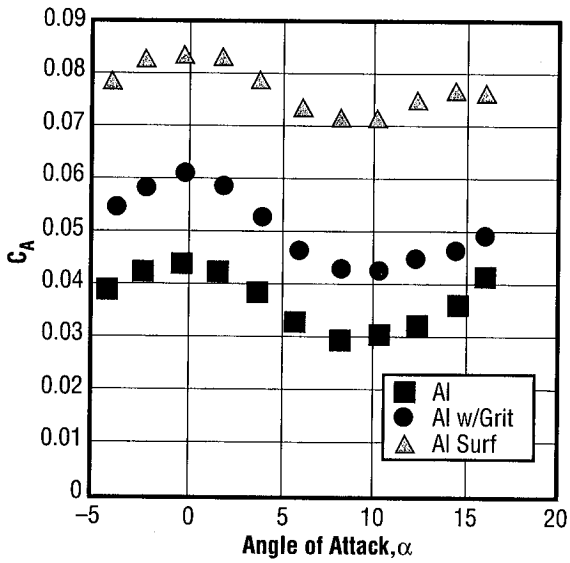

FIGURE 90.—Comparison of axial force coefficient at Mach 0.8.

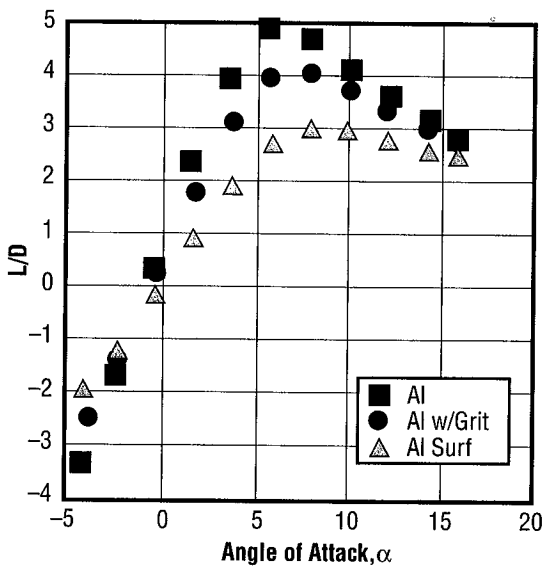

FIGURE 91.—Comparison of lift over drag at Mach 0.8.

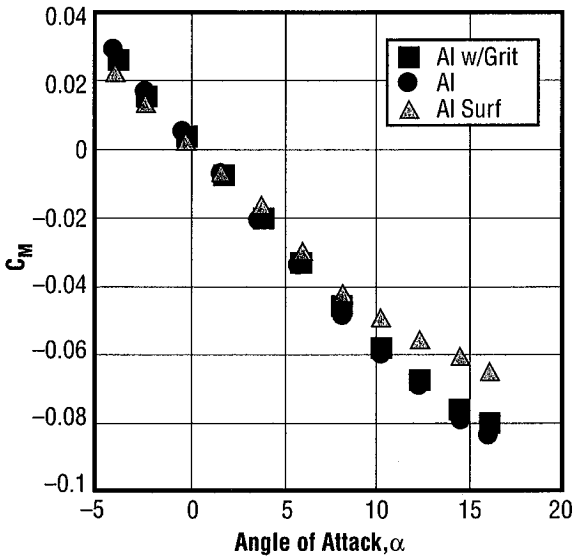

FIGURE 92.—Comparison of pitching moment coefficient at Mach 1.05.

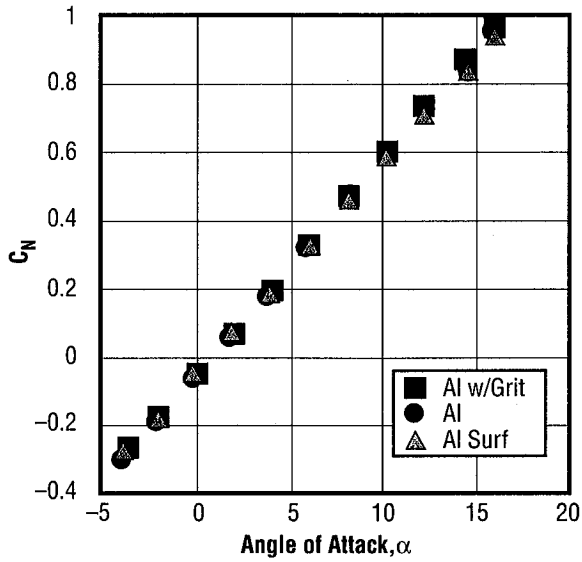

FIGURE 93.—Comparison of normal force coefficient at Mach 1.05.

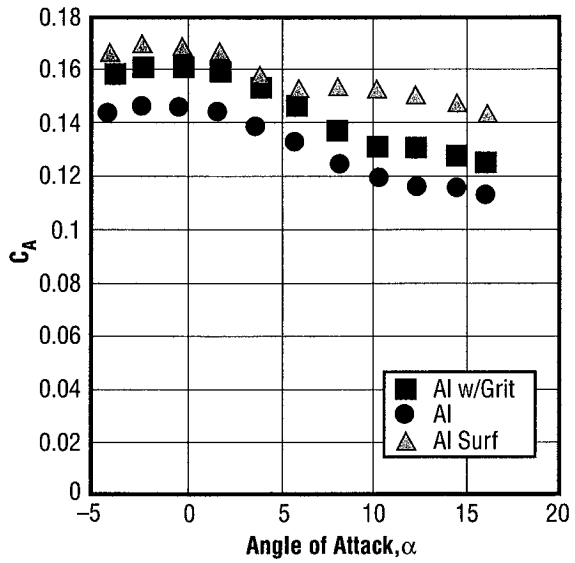

FIGURE 94.—Comparison of axial force coefficient at Mach 1.05.

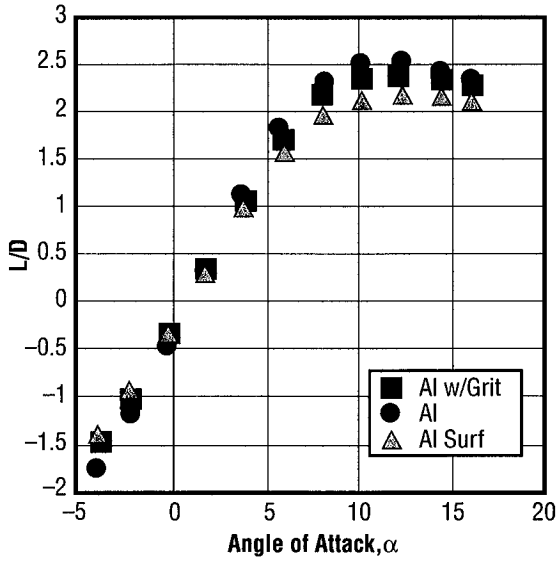

FIGURE 95.—Comparison of lift over drag at Mach 1.05.

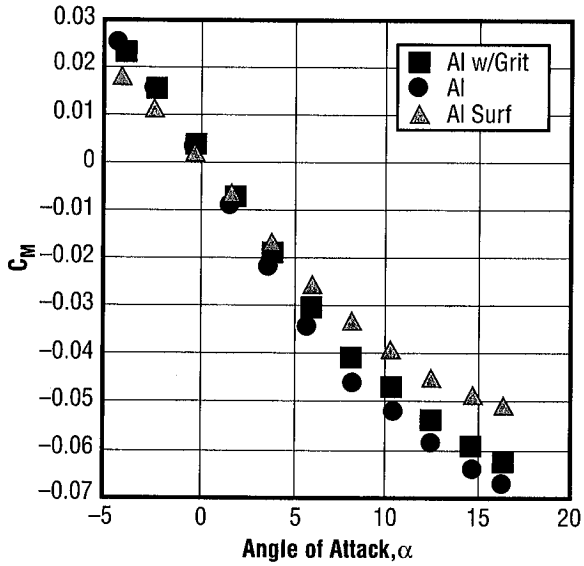

FIGURE 96.—Comparison of pitching moment coefficient at Mach 1.2.

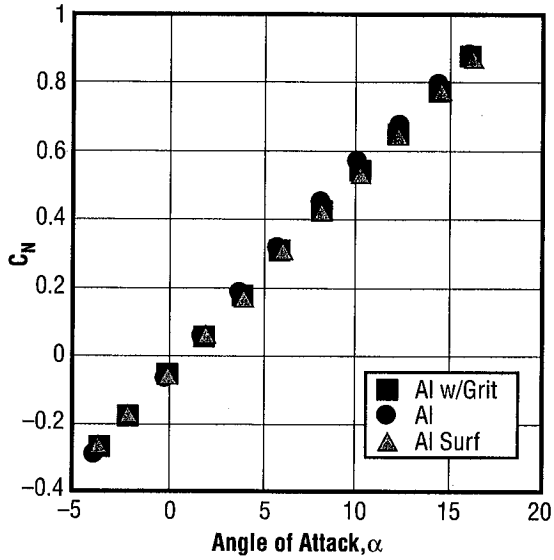

FIGURE 97.—Comparison of normal force coefficient at Mach 1.2.

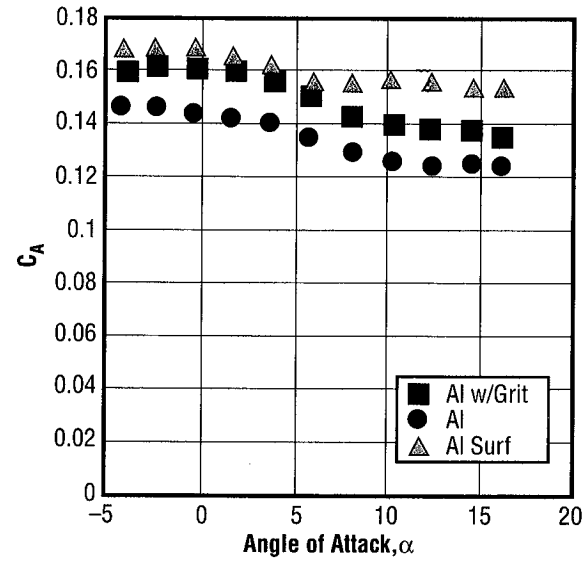

FIGURE 98.—Comparison of axial force coefficient at Mach 1.2.

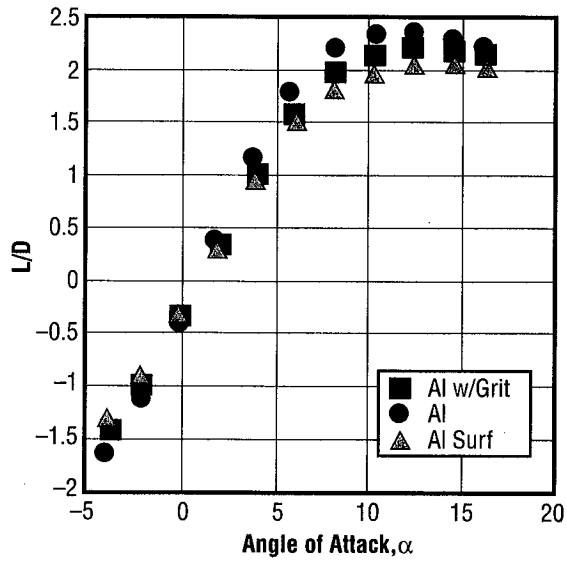

FIGURE 99.—Comparison of lift over drag at Mach 1.2.

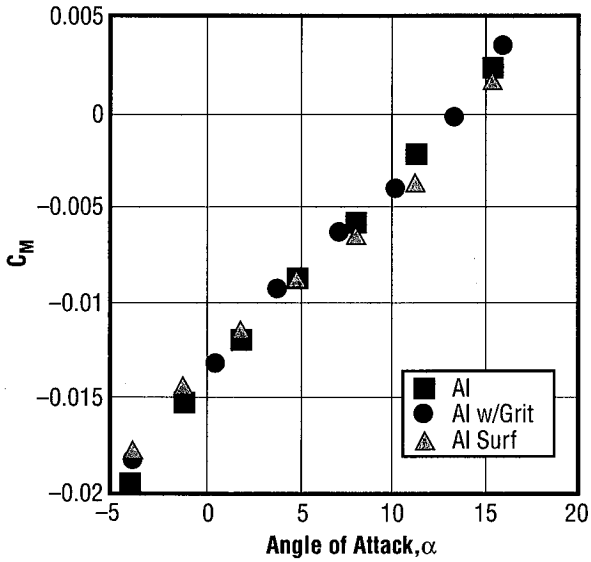

FIGURE 100.—Comparison of pitching moment coefficient at Mach 3.48.

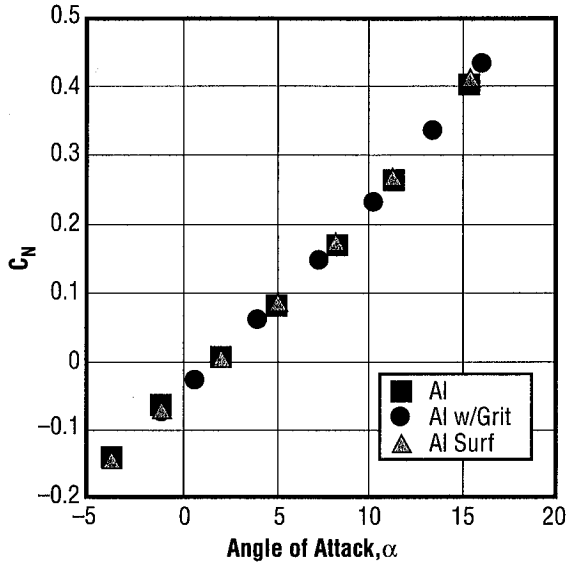

FIGURE 101.—Comparison of normal force coefficient at Mach 3.48.

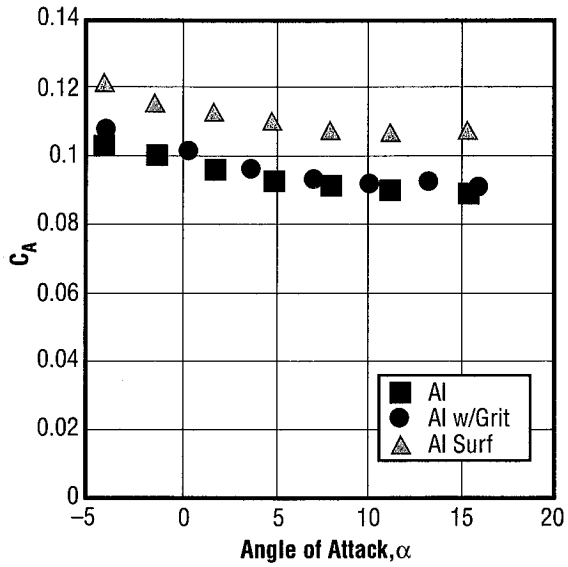

FIGURE 102.—Comparison of axial force coefficient at Mach 3.48.

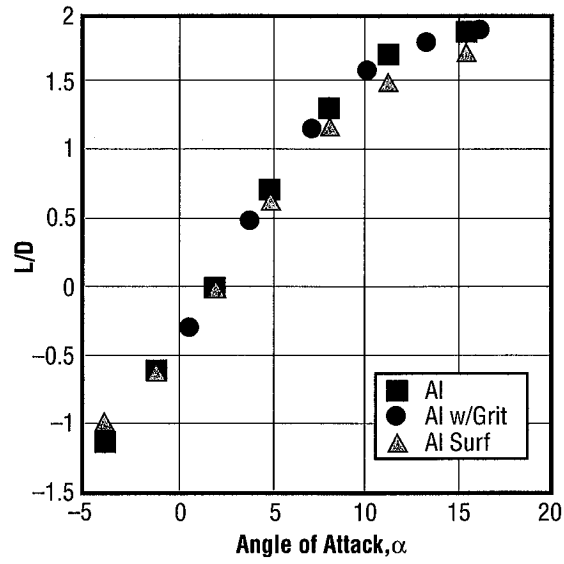

FIGURE 103.—Comparison of lift over drag at Mach 3.48.

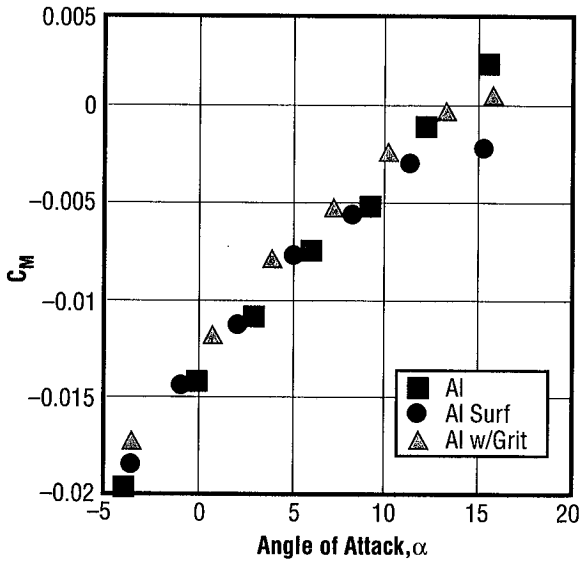

FIGURE 104.—Comparison of pitching moment coefficient at Mach 4.96.

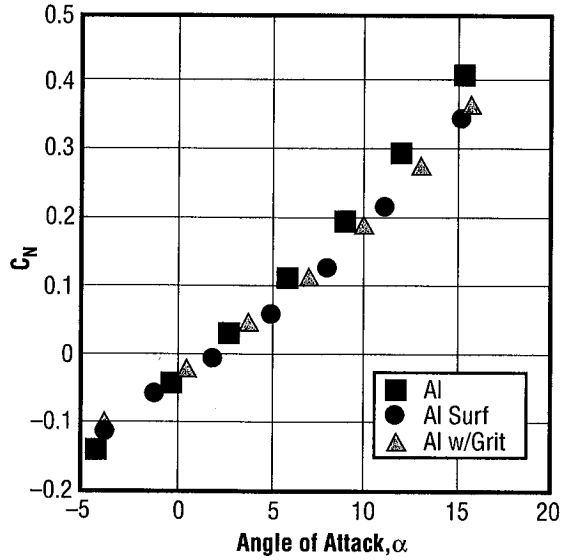

FIGURE 105.—Comparison of normal force coefficient at Mach 4.96.

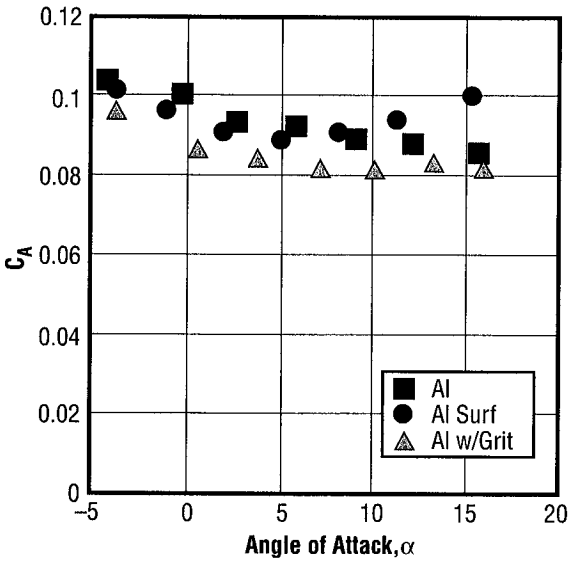

FIGURE 106.—Comparison of axial force coefficient at Mach 4.96.

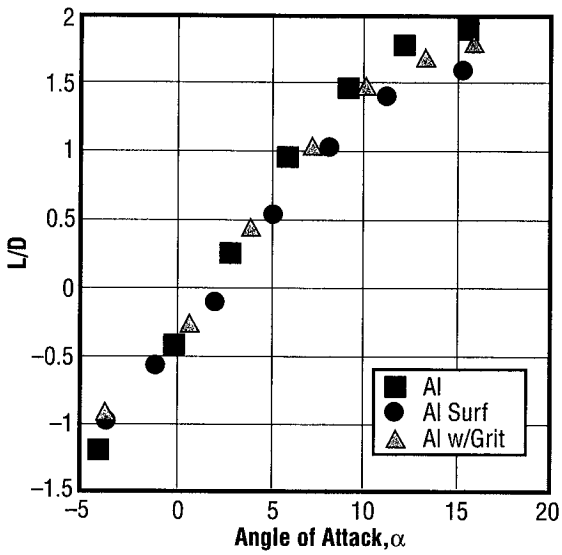

FIGURE 107.—Comparison of lift over drag at Mach 4.96.

4. Cost and Time

The cost and time requirements for the various RP models and the metal model are shown in table 4. The RP models for this test cost about $3,000 and took between 2 and 3 weeks to construct, while the metal or aluminum model cost about $15,000 and took 3 1/2 months to design and fabricate. At the time of this study, MSFC had in-house capabilities to produce FDM and SLA models, and these capabilities were utilized. The costs are from quotes given by various secondary sources that specialize in RP part fabrication. It should be noted that the latest quote for the conversion of an RP model to wind tunnel model is $600—$100 for the balance adapter and $500 for parts and labor. This was quoted as taking 2 work days. Along with the standard 3 days for RP model fabrication, a wind tunnel model could be constructed in under a week. These data are shown in table 5. At the time of writing this report, MSFC has the in-house capability to construct models using all the RP processes reported in this publication.

TABLE 4.—*Wind tunnel model time and cost summary.*

Model Cost and Time (Time and cost for test models)	**SLA**	**FDM–ABS**	**LOM**	**SLS**	**Aluminum**
RP Model	$1,200	$1,000	$ 900	$1,400	
Conversion	2,000	2,000	2,000	2,000	
Balance Adapter	100	100	100	100	
Total Cost	$3,300	$3,100	$3,000	$3,500	$15,000
Time	2–3 Weeks	2–3 Weeks	2–3 Weeks	2–3 Weeks	3 1/2 Months

TABLE 5.—*Current RP wind tunnel model time and cost.*

RP Model	*$ 500
Conversion	500
Balance Adapter	100
Cost	$1,100
Time	1–2 Weeks

* All processes can be done inhouse at MSFC incurring materials costs only, approximately $500.

VII. ACCURACY

A. Precursor Study

The data accuracy resulting from the precursor test can be divided into two sources of error or uncertainty: (1) the model, and (2) the data acquisition system. Each of these factors will be considered. First, the dimensions of the two models must be considered. Difficulty arose in the interface between the nose and core body for the RP model along with the roll of the balance adapter in the model. A comparison of model dimensions is shown in table 6. Other discrepancies in the RP model dimensions were that the flat sides of the base varied within 0.005 inch, and the diameter at the nose junction did not vary linearly due to smoothing the model for a good fit between the nose and core body.

TABLE 6.—*Vertical lander model dimensions (inches).*

Dimension	Steel	FDM
Length	9.001	9.007
Width	2.504	2.513
Height	2.500	2.516

The RP model's balance adapter was rolled in the model with respect to the metal model approximately 2.5 degrees. The RP model's balance adapter was rolled approximately 2 degrees starboard wing down, while the metal model's balance adapter was rolled approximately 0.5 degree port wing down, resulting in a difference of approximately 2.5 degrees between the two models. This resulted in a small error in all the coefficients, since the model was installed in the tunnel level. The effect of the balance adapter roll on the normal force and side force aerodynamic coefficients is shown in table 7 if a C_N of 1.0 and a C_Y of 0.0 are assumed.

TABLE 7.—*Effect of balance adapter roll on aerodynamic coefficients.*

Roll Angle	C_N	C_Y
0.5°	0.9999	0.0087
1.0°	0.9998	0.0175
1.5°	0.9997	0.0262
2.0°	0.9994	0.0349
2.5°	0.9990	0.0436
		(Factor of C_N)

The repeatability of the data can be considered to be within the symbol size on the plots. The capacity and accuracy for the balance used during this test are given in table 8. Table 9 lists the aerodynamic coefficient uncertainty for the vertical lander models.

TABLE 8.—*Balance 250 capacity and accuracy.*

	Capacity	Accuracy
Normal Force	200 lb	±0.20 lb
Side Force	107 lb	±0.50 lb
Axial Force	75 lb	±0.25 lb
Pitching Moment	200 in-lb	±0.20 in-lb
Rolling Moment	50 in-lb	±0.25 in-lb
Yawing Moment	107 in-lb	±0.50 in-lb

TABLE 9.—*Vertical lander aerodynamic coefficient uncertainty.*

Mach	Coefficient Accuracy Capacity Q (lb/in^2)	C_N 0.2 200 lb	C_M 0.2 200 in-lb	C_Y 0.5 107 lb	C_{YN} 0.5 107 in-lb	$C_{\ell\beta}$ 0.25 50 lb	C_A 0.25 75 lb
0.2	0.6	0.06724497	0.00747166	0.16811243	0.01867916	0.00933958	0.08405622
0.3	1.3	0.03103614	0.00344846	0.07759035	0.00862115	0.00431058	0.03879518
0.6	4.36	0.0092539	0.00102821	0.02313474	0.00257053	0.00128526	0.01156737
0.8	6.47	0.00623601	0.00069289	0.01559002	0.00173222	0.00086611	0.00779501
0.9	7.36	0.00548193	0.0006091	0.01370482	0.00152276	0.00076138	0.00685241
0.95	7.76	0.00519935	0.00057771	0.01299838	0.00144426	0.00072213	0.00649919
1.05	8.48	0.0047579	0.00052866	0.01189475	0.00132164	0.00066082	0.00594737
1.1	8.76	0.00460582	0.00051176	0.01151455	0.00127939	0.0006397	0.00575728
1.15	8.99	0.00448798	0.00049866	0.01121996	0.00124666	0.00062333	0.00560998
1.25	9.31	0.00433373	0.00048153	0.01083431	0.00120381	0.00060191	0.00541716
1.46	9.49	0.00425153	0.00047239	0.01062882	0.00118098	0.00059049	0.00531441
1.96	11.00	0.00366791	0.00040755	0.00916977	0.00101886	0.00050943	0.00458488
2.74	6.38	0.00632398	0.00070266	0.01580995	0.00175666	0.00087833	0.00790497
3.48	5.15	0.00783437	0.00087049	0.01958591	0.00217621	0.00108811	0.00979296
4.96	2.73	0.01477912	0.00164212	0.03694779	0.00410531	0.00205265	0.01847389

S_{ref} 4.957 in^2
L_{ref} 9.00 in

The greatest source of uncertainty for this test was in the axial force correction for the model weight tare. Initially, due to time constraints, the weight tare of the metal model was used during testing for the RP model. After the test, the actual weight tare of the RP model was determined. Correcting the data for this tare resulted in assumptions being made because some of the initial parameters used in the actual weight tare calculation were not known. Uncertainty and possible error in this correction can account for 25 percent of the difference between the axial force data of the RP and metal models.

B. Baseline Study

The data accuracy results from this test can be divided into two sources of error or uncertainty: (1) the model, and (2) the data acquisition system. Each of these factors will be considered separately.

First, the dimensions of each model must be compared. Difficulty arose in the interface between the nose and core body for the RP models, along with the roll of the balance adapter in the models. Also the contours of the models used in this test were measured at two wing sections, vehicle stations, tail sections, and the XY and XZ planes. A comparison of model dimensions is shown in table 10. Two sectional cuts were made on each wing, left and right; two on the body; two on the vertical tail, and one cut in the XY and XZ planes. This shows a representation of the maximum discrepancy in model dimensions relative to the baseline CAD model used to construct all the models at each given station. The standard model tolerance is 0.005 inch.

TABLE 10.—*Model dimensions compared to theoretical (inches).*

Δ Wing-Body Model Dimensions (in)					
	AL	SLS*	SLA	FDM	SLS 2
Wing L1	0.0097	0.0117	0.0067	0.0087	0.0091
Wing L2	0.0043	0.0157	0.0049	0.0065	0.0159
Wing R1	0.0042	0.0102	0.0053	0.0028	0.0189
Wing R2	0.0054	0.0087	0.006	0.0043	0.0149
Body 1	0.007	0.0043	0.0028	0.0144	0.0046
Body 2	0.0019	0.012	0.0055	0.012	0.0055
Tail 1	0.0031	0.0102	0.0044	0.0031	0.0094
Tail 2	0.002	0.01	0.0029	0.0028	0.0051
XY Plane	0.0012	0.0031	0.0299	0.0065	0.0093
XZ Plane	0.003	0.0176	0.0251	0.0546	0.024

*Post-processing problem with wing and tail

The installation of the balance adapter in both the metal and RP models was not at 0 degrees roll (noted in table 11).

TABLE 11.—*Balance adapter roll angle.*

Balance Adapter Roll Angle Installed in Model	
Model	Adapter Roll Angle (Deg)
AI	0.95
SLA	2.25
SLS	1.05
FDM–ABS	1.57
SLS #2	1.20

The metal model's balance adapter was rolled approximately 1 degree starboard wing down, while the RP models were rolled from 1 degree to 2.25 starboard wing down, resulting in a difference of approximately 0 degrees to 1.25 degrees between the two models. This resulted in a small error in all the coefficients, since the model was installed in the tunnel level. The effect of the balance adapters roll on the normal force and side force aerodynamic coefficients is shown in table 7.

Second, the repeatability of the data can be expected to be within the symbol size on the plots. Also, the capacity and accuracy for the balance used during this test is given in table 8. Table 12 lists the aerodynamic coefficient uncertainty for the wing-body models.

TABLE 12.—*Aerodynamic coefficient uncertainty for the wing-body models.*

Mach	Coefficient Accuracy Capacity Q (lb/in^2)	C_N 0.2 200 lb	C_M 0.2 200 in-lb	C_Y 0.5 107 lb	C_{YN} 0.5 107	$C_{\ell\beta}$ 0.25 50 lb	C_A 0.25 75 lb
0.2	0.6	0.03840246	0.00430424	0.09600614	0.01076061	0.0053803	0.04800307
0.3	1.3	0.01772421	0.00198657	0.04431053	0.00496643	0.00248322	0.02215526
0.6	4.36	0.00528474	0.00059233	0.01321185	0.00148082	0.00074041	0.00660593
0.8	6.47	0.00356128	0.00039916	0.0089032	0.00099789	0.00049895	0.0044516
0.9	7.36	0.00313064	0.00035089	0.00782659	0.00087722	0.00043861	0.00391329
0.95	7.76	0.00296926	0.0003328	0.00742316	0.00083201	0.000416	0.00371158
1.05	8.48	0.00271716	0.00030455	0.00679289	0.00076136	0.00038068	0.00339644
1.1	8.76	0.00263031	0.00029481	0.00657576	0.00073703	0.00036851	0.00328788
1.15	8.99	0.00256301	0.00028727	0.00640753	0.00071817	0.00035909	0.00320376
1.25	9.31	0.00247492	0.00027739	0.00618729	0.00069349	0.00034674	0.00309365
1.46	9.49	0.00242797	0.00027213	0.00606994	0.00068033	0.00034017	0.00303497
1.96	11.00	0.00209468	0.00023478	0.0052367	0.00058694	0.00029347	0.00261835
2.74	6.38	0.00361152	0.00040479	0.00902879	0.00101197	0.00050598	0.0045144
3.48	5.15	0.00447407	0.00050147	0.01118518	0.00125366	0.00062683	0.00559259
4.96	2.73	0.0084401	0.00094599	0.02110025	0.00236497	0.00118248	0.01055013

S_{ref} 8.68 in^2
L_{ref} 8.922 in

VIII. CONCLUSIONS

A. Precursor Study

It can be concluded from this precursor test that wind tunnel models constructed using rapid prototyping methods and materials can be used in subsonic, transonic, and supersonic wind tunnel testing for initial baseline aerodynamic database development. The accuracy of the data is lower than that of a metal model due to surface finish and dimensional tolerances, but is quite accurate for this level of testing. The under 5 percent change in the aerodynamic data between the metal and RP model aerodynamics is acceptable for this level of preliminary design or phase A/B studies. The use of RP models will provide a rapid capability in the determination of the aerodynamic characteristics of preliminary designs over a large Mach range. This range covers the transonic regime, a regime in which analytical and empirical capabilities sometimes fall short.

B. Baseline Study

Rapid prototyping methods have been shown to be feasible in their limited direct application to wind tunnel testing for producing preliminary aerodynamic databases. Cost savings and model design/fabrication time reductions of over a factor of 4 have been realized for RP techniques as compared to current standard model design/fabrication practices. This makes wind tunnel testing more affordable for small programs with low budgets and for educational purposes. From this project MSFC has gained a greater capability for a quick turnaround on wind tunnel testing for high-priority programs, which can result in higher fidelity aerodynamic databases earlier in the preliminary phases of launch vehicle design. At this time, RP methods and materials can be used for only preliminary design studies and limited configurations due to the rapid prototyping material properties which allow bending of model components under high loading conditions (i.e., high angles-of-attack).

This test initially indicated that two of the RP methods were not mature enough to produce an adequate model. These methods were FDM using PEEK and LOM using plastic. The "paper" LOM model did not have adequate material properties to withstand the conversion process to a wind tunnel model. The other three processes and materials produced satisfactory models which were successfully tested. The initial SLS model did not produce good results due to problems with tolerances in post-processing. This was corrected in the second model which produced satisfactory results, but not as good as FDM or SLA. FDM–ABS and SLA produced very good results for model replacement parts. The data resulting from the FDM–ABS model diverged at higher loading conditions producing unsatisfactory results. It should be noted that this material/process produced satisfactory results over the full range of test conditions for the vertical lander configuration tested in the precursor study. SLA was shown to be the best RP process with satisfactory results for a majority of the test conditions. The differences between the configurations data can be attributed to multiple factors such as surface finish, structural deflection, and tolerances on the fabrication of the models when they are "grown."

It can be concluded from this study that wind tunnel models constructed using rapid prototyping methods and materials can be used in subsonic, transonic, and supersonic wind tunnel testing for initial baseline aerodynamic database development. The accuracy of the data is lower than that of a metal model due to surface finish and dimensional tolerances, but is quite accurate for this level of testing. The difference in the aerodynamic data between the metal and RP model aerodynamics is acceptable for this level of preliminary design or phase A/B studies. The use of RP models will provide a rapid capability in the determination of the aerodynamic characteristics of preliminary designs over a large Mach range. This range covers the transonic regime, a regime in which analytical and empirical capabilities sometimes fall short.

However, at this time, replacing machined metal models with RP models for detailed parametric aerodynamic and control surface effectiveness studies is not considered practical because of the high configuration fidelity required and the loads that deflected control surfaces must withstand. The current plastic materials of RP models may not provide the structural integrity necessary for survival of thin section parts such as tip fins and control surfaces. Consequently, while this test validated that RP models can be used for obtaining preliminary aerodynamic databases, further investigations will be required to prove that RP models are adequate for detailed parametric aerodynamic studies that require deflected control surfaces and delicate or fragile fins.

BIBLIOGRAPHY

Jacobs, P.F.: "Stereolithography and Other RP&M Technologies." ASME Press, 1996.

Springer, A.; and Cooper, K.: "Application of Rapid Prototyping Methods to High-Speed Wind Tunnel Testing." Proceedings of 86th Semiannual Meeting Supersonic Tunnel Association October 1996.

Springer, A.; Cooper, K.; and Roberts, F.: "Application of Rapid Prototyping Models to Transonic Wind Tunnel Testing." AIAA 97–0988, 35th Aerospace Sciences Meeting. January 1997.

Springer, A.; and Cooper, K.: "Comparing the Aerodynamic Characteristics of Wind Tunnel Models Produced by Rapid Prototyping and Conventional Methods." AIAA 97–2222, 15th AIAA Applied Aerodynamics Conference, June 1997.

REPORT DOCUMENTATION PAGE

Form Approved
OMB No. 0704-0188

1. AGENCY USE ONLY *(Leave Blank)*	2. REPORT DATE	3. REPORT TYPE AND DATES COVERED
	May 1998	Technical Publication

4. TITLE AND SUBTITLE
Application of Rapid Prototyping Methods to High-Speed Wind Tunnel Testing (MSFC Center Director's Discretionary Fund Final Report, Project No. 96–21)

5. FUNDING NUMBERS

6. AUTHORS
A.M. Springer

7. PERFORMING ORGANIZATION NAMES(S) AND ADDRESS(ES)
George C. Marshall Space Flight Center
Marshall Space Flight Center, Alabama 35812

8. PERFORMING ORGANIZATION REPORT NUMBER
M–870

9. SPONSORING/MONITORING AGENCY NAME(S) AND ADDRESS(ES)
National Aeronautics and Space Administration
Washington, DC 20546–0001

10. SPONSORING/MONITORING AGENCY REPORT NUMBER
NASA TP–1998–208396

11. SUPPLEMENTARY NOTES
Prepared by the Structures and Dynamics Laboratory, Science and Engineering Directorate

12a. DISTRIBUTION/AVAILABILITY STATEMENT
Unclassified–Unlimited
Subject Category 02
Standard Distribution

12b. DISTRIBUTION CODE

13. ABSTRACT *(Maximum 200 words)*

This study was undertaken in MSFC's 14-Inch Trisonic Wind Tunnel to determine if rapid prototyping methods could be used in the design and manufacturing of high speed wind tunnel models in direct testing applications, and if these methods would reduce model design/fabrication time and cost while providing models of high enough fidelity to provide adequate aerodynamic data, and of sufficient strength to survive the test environment. Rapid prototyping methods utilized to construct wind tunnel models in a wing-body-tail configuration were: fused deposition method using both ABS plastic and PEEK as building materials, stereolithography using the photopolymer SL–5170, selective laser sintering using glass reinforced nylon, and laminated object manufacturing using plastic reinforced with glass and "paper."

This study revealed good agreement between the SLA model, the metal model with an FDM–ABS nose, an SLA nose, and the metal model for most operating conditions, while the FDM–ABS data diverged at higher loading conditions. Data from the initial SLS model showed poor agreement due to problems in post-processing, resulting in a different configuration. A second SLS model was tested and showed relatively good agreement. It can be concluded that rapid prototyping models show promise in preliminary aerodynamic development studies at subsonic, transonic, and supersonic speeds.

14. SUBJECT TERMS	15. NUMBER OF PAGES
rapid prototyping, wind tunnel testing, launch vehicle aerodynamics	60
	16. PRICE CODE A04

17. SECURITY CLASSIFICATION OF REPORT	18. SECURITY CLASSIFICATION OF THIS PAGE	19. SECURITY CLASSIFICATION OF ABSTRACT	20. LIMITATION OF ABSTRACT
Unclassified	Unclassified	Unclassified	Unlimited